Fluorescent Biological Aerosol Particle Measurements at a Tropical High Altitude Site in Southern India during Southwest Monsoon Season

A. E. Valsan[1,*], R. Ravikrishna[2], C. V. Biju[3], C. Pöhlker[4], V. R. Després[5], J. A. Huffman[6], U. Pöschl[7], and S. S. Gunthe[1,**]

[1]EWRE Division, Department of Civil Engineering, Indian Institute of Technology Madras, Chennai – 600 036, India.

[2]Department of Chemical Engineering, Indian Institute of Technology Madras, Chennai – 600 036, India.

[3]Department of Civil Engineering, College of Engineering Munnar, PB.No:45, County Hills, Munnar – 685612, India.

[4]Biogeochemistry Department, Max Planck Institute for Chemistry, P. O. Box Number 3060, Mainz, Germany.

[5]Institute of General Botany, Johannes Gutenberg University, Mainz, Germany.

[6]Department of Chemistry and Biochemistry, University of Denver, 2190 E. Iliff Ave., Denver, CO, 80208, USA.

[7]Multiphase Chemistry Department, Max Planck Institute for Chemistry, P. O. Box 3060, Mainz, Germany

To whom correspondence should be addressed:

[*]Aswathy E. Valsan (aswathyerat@gmail.com)

[**]Sachin S. Gunthe (s.gunthe@iitm.ac.in)

Abstract

An ultraviolet aerodynamic particle sizer (UV-APS) was continuously operated for the first time during two seasons to sample the contrasting winds during monsoon and winter to characterize the properties of fluorescent biological aerosol particles (FBAPs), at a high altitude site in India. Averaged over the entire monsoon campaign (June 1, 2014 – August 21, 2014) the arithmetic mean number and mass concentrations of coarse-mode (>1 μm) FBAP were 0.02 cm^{-3} and 0.24 μg m^{-3}, respectively, which corresponded to ~2 and 6 % of total aerosol loading, respectively. Average FBAP number size distribution exhibited a peak at ~3 μm, which is attributed to the fungal spores, as supported by scanning electron microscope (SEM) images, and these results are consistent with previous studies made for FBAP. During eleven weeks of measurements the variability of the total coarse mode particle number (TAP) concentration was high compared to that observed in FBAP number concentration. The TAP and FBAP number concentrations measured at this site were strongly dependent on changes in wind direction and rainfall. During periods of westerly/southwesterly winds with heavy persistent rainfall, the TAP and FBAP concentration exhibited very low values (1.3 cm^{-3} and 0.005 cm^{-3}, respectively) with no significant diurnal variations. Whereas during periods of Northerly winds with scattered rainfall FBAP exhibited relatively high concentration values (0.05 cm^{-3}) with pronounced diurnal variations, which were strongly coupled with diurnal variations in meteorological parameters. The campaign averaged FBAP number concentrations were shown to correlate with daily patterns of meteorological parameters and were positively correlated with relative humidity (RH; R^2=0.58), and negatively with temperature (R^2=0.60) and wind speed (R^2=0.60). We did not observe any significant positive correlation with precipitation as reported by previous researchers from selected areas. These measurement results confirm the fact that the ratio of PBAPs to TAP

48 is strongly dependent on particle size and location and thus may constitute a significant
49 proportion of total aerosol particles.

1 Introduction

Aerosols are generally defined as a colloidal system of solid or liquid particles suspended in a gaseous medium (Fuzzi et al., 1997; Pöschl, 2005) and are ubiquitous in the Earth's atmosphere. The term "Primary Biological Aerosol Particles" (PBAPs; sometimes also referred as bioaerosols or biological aerosols), describes a subset of solid airborne particles originating from biological organisms, including viruses, pollen, microorganisms (bacteria, fungal spores, etc.) and, protozoa or algae, etc., together with fragments of biological materials such as animal dander, plant debris etc. (Artaxo and Hansson, 1995; Coz et al., 2010; Després et al., 2007, 2012; Elbert et al., 2007). Bioaerosols can range in size from a few nanometers to few hundred micrometers in aerodynamic diameter, D_a, (Coz et al., 2010; Després et al., 2012; Jones and Harrison, 2004; Matthias-Maser and Jaenicke, 1994). PBAPs have been shown to constitute 14 – 70% of total number of coarse mode particles and around 20 – 24 % of total mass of PM_{10} (particulate matter with size ≤10 μm; Elbert et al., 2007; Després et al., 2012; Pöschl et al., 2010; Huffman et al., 2012). Further, it is likely that the surface structure, ice nucleating proteins, and other characteristics of bioaerosols can influence the heterogeneous ice nuclei formation at relatively high temperature levels (Morris et al., 2004, 2014). Bioaerosols can thus act as giant cloud condensation nuclei (GCCN), thus affecting the hydrological cycle (Andreae and Rosenfeld, 2008; Möhler et al., 2007). It is also known that pollen and spores associated with various plants and fungi are dispersed in air resulting in the distribution and transfer of genetic material over large distances (Huffman et al., 2010; Elbert et al., 2007; Hallar et al., 2011; Burrows et al., 2009). A side effect of such transport and distribution is that they can play a negative role in public health. Pathogenic fungi have long been recognized as major threats to animal health and

plants including crops severely jeopardizing the food security (Fisher et al., 2012 and references therein).

The last decade has experienced a substantial development and application of advanced online and offline techniques for studying the characteristic properties of bioaerosols in both field and laboratory (Fröhlich-Nowoisky, et al., 2009; DeLeon-Rodriguez et al., 2013; Prenni et al., 2009; Huffman et al., 2010, 2012, 2013; Schumacher et al., 2013; Pöhlker et al., 2012, 2013). Instruments utilizing laser-induced fluorescence (LIF) have been frequently deployed in the field, enabling real-time characterization of the number size distribution of PBAPs with high time and size resolution. However, instruments based on LIF do not provide detailed information directly about PBAPs or the origin of particles, but provide broadly categorized information due to a mixture of biological fluorophores, each detected with varying efficiency (Pohlker et al., 2012, 2013). Most FBAP measurements have shown that the dominant size range for PBAPs number size distribution is 1 – 4 μm with concentration varying within the factor of 10 (Gabey et al., 2011, 2013; Healy et al., 2014; Huffman et al., 2010, 2012, 2013; Saari et al., 2015; Schumacher et al., 2013; Toprak and Schnaiter, 2013; Yu et al., 2016). As studied and described by Huffman et al., (2010), based on four months of measurements in central Europe, the signal detected by UV-APS (Ultraviolet Aerodynamic Particle Sizer) was defined as Fluorescent Biological Aerosol Particles (FBAP). Hence, the term FBAP is used as a lower limit proxy for primary biological aerosol particles (PBAPs), biological aerosols, biological aerosol particles, bioaerosols and similar terms mentioned in this study.

Despite such instrumental advancements described above, studies related to the quantification of bioaerosols and their role in climate and human health have been extremely limited in space and time. This is particularly true for the Indian subcontinent, which constitute ~18% of the world's

total population, where studies related to the bioaerosols are relatively few and with analysis performed only by traditional techniques (Bhati and Gaur, 1979; Chakraborty et al., 1998; Gangamma, 2014; Srivastava et al., 2012; Sharma and Rai, 2008; Pachauri et al., 2013; Valsan et al., 2015; Ansari et al., 2015; Adhikari et al., 2004). The abundance of bioaerosols, which is strongly dependent on location and season, remains poorly characterized over the Indian subcontinent and need to be addressed systematically.

Additionally, investigating and quantifying the role of bioaerosols over the Indian continent is important due to its diverse land-use pattern and the unique climatic condition experienced in terms of two monsoon seasons associated with two distinct synoptic scale wind patterns. The concentration of fluorescent aerosol particles in a semi-arid forest in the Western US was shown to increase during and after rainfall (Huffman et al., 2013). Rainfall-triggered increase in bioaerosol concentration can potentially enhance further precipitation by convective upward movement of bioaerosols into clouds where they can serve either as IN or giant CCN (Shcumacher et al., 2013; Huffman et al., 2013). Thus, the bioaerosols emitted during monsoon rainfall could potentially play an important role in cloud and precipitation formation over India (Ansari et al., 2015).

Therefore, it is very important to understand and quantify the role of bioaerosols in cloud and precipitation formation during monsoon and convective rainfall. Additionally, bioaerosols over the Indian sub-continent can directly impact society through the spread of diseases and indirectly due to increased risk of loss of agricultural output due to emerging diseases caused by the fungi (Fisher et al., 2012).

Studies involving characterization of bioaerosols using advanced techniques over this region are important to understand and quantify the impact of bioaerosols on regional biodiversity with

larger implication towards human and ecosystem health. With this motivation we have deployed a UV-APS for the detection and measurement of number size distribution of PBAPs at a high-altitude site of Munnar in Western Ghats of southern tropical India during Southwest monsoon season for ~3 months. To our knowledge this study presents the first ambient measurement investigation involving UV-APS for multiple months over the Indian subcontinent.

2 Methods

2.1 Site Description

Measurements were performed to sample the air masses (see section 2.2) from a high-altitude site (Munnar; 10.09°N, 77.06°E; 1605 m amsl – above mean sea level – Fig. 1) located in the Western Ghats region of Southern, tropical India, just 90 km away from the Arabian Sea. The observational site is located on a hill with a valley towards the South and a small mountain towards the North surrounded by dense vegetation including tea gardens and Eucalyptus trees. Climatologically this region is classified as subtropical highland with dry winters and is listed as the Shola forest-grass ecosystem as defined in the land-use type terminology (Fig. S1). The Western Ghats, one of the eight mountain ranges in India and identified as one of the most significant hot spots of biodiversity (Myers et al., 2000) in the world, originates near the border of Maharashtra and Gujarat running ~1600 km towards South, parallel to the Western coast through the states of Gujarat, Maharashtra, Karnataka, Kerala, and Tamilnadu ending at the Southern tip of India near Kanyakumari. This mountain range separates the coastal plain from the Deccan plateau making Western coastal plain a narrow land strip with a maximum width of ~ 110 – 120 km, sandwiched between the Western Ghats and the Arabian Sea. During the SW Monsoon season (June – September) the Southwesterly, moisture laden winds are intercepted by

the Western Ghats causing persistent and heavy rainfall on the windward side of these mountains. This causes the wash out and wet deposition of the pollutants in the coastal strip (Kerala) emitted due to anthropogenic activities, thus bringing clean marine influx with minimum impact of anthropogenic emissions (Satheesh and Srinivasan, 2002). Therefore, during this particular season this observational site can be regarded as relatively pristine, as compared to any other operational high-altitude observatory/site in Indian tropical region (Shika et al., 2016).

2.2 General Meteorology

Southern India nominally experiences two Monsoon seasons, the SW monsoon and the Northeast monsoon (NE; November – January), which are strongly associated with the movement of Inter-Tropical Convergence Zone, the ITCZ (Kanawade et al., 2014). The SW monsoon winds bring relatively clean marine influx over the continent from Arabian Sea when the ITCZ moves Northwards reaching 30°N during July (Naja and Lal, 2002). These air masses originate over the Indian Ocean and travel thousands of kilometers over the ocean, including the Arabian Sea, before reaching the observational site. The Southward movement of ITCZ reaching up to the equator is associated with the NE monsoon, which is also marked as winter season in India occurring during October to January, when the prevailing winds are predominantly blowing in the NE direction. The measurement site of Munnar receives more than 85% of its annual rainfall during SW monsoon season and experiences scattered rainfall events during NE monsoon. The detailed meteorological parameters measured during the field measurement campaign carried out during SW Monsoon season at Munnar are discussed below.

2.3 Real-time fluorescence measurement

Biological aerosol particles at Munnar were measured using a UV-APS (TSI Inc. Model 3314) as per the standard instructions given in the technical manual. The detailed description about the instrument including operating principles, field operation, data analysis protocol, and critical operational parameters are discussed elsewhere (Kanaani, et al., 2007, 2008; Agranovski et al., 2003, 2004, 2005; Brosseau et al., 2000; Huffman et al., 2010, 2012; Hairston et al., 1997).

Briefly, the instrument is capable of measuring aerosol particles in the aerodynamic diameter (D_a) range of 0.5 – 20 μm over 52 channels by measuring the time-of-flight of particles between two He-Ne red lasers (λ=633 nm). Once the particle size is determined, each particle is excited using an ultraviolet Nd:YAG laser (λ=355 nm) and fluorescent emission is measured in the range of 420 – 575 nm. The spectrally unresolved total fluorescence is recorded for each individual particle in to one of 64 channels. The UV-APS measurements were obtained at 5 minutes interval (recording a total of 22280 sampling points during entire measurement campaign) with a volumetric flow rate of 5 Lpm at ambient temperature and pressure. All times reported in this study were Indian Standard Time (IST).

Sampling was performed at a building of the College of Engineering, Munnar, Kerala. The sampling inlet was approximately 2 m above the rooftop of the building and 8 m above the ground level. The sampling inlet was connected to the UV-APS, which was placed next to the window inside a room using 3m of ¾" OD stainless steel tubing. To minimize the particle losses, due to impaction resulting from sharp bends, electrically conductive silicon rubber tubing (~1.5 m; 12 mm inner diameter) was attached to the stainless steel tube just outside the window (Fig. S1). The air sample was passed through a diffusion dryer (~1 m length) with silica gel before entering the UV-APS, thus maintaining the relative humidity of inlet air to <40%.The residence time of sampled air in the inlet tube was calculated to be ~ 20 seconds, and the flow was

calculated to be laminar in the entire sampling line. Hence, diffusion losses were expected to be negligible for all the size-ranges of the sampled particles (average penetration efficiency of 99.8% at 290K and 840 hPa; Baron and Willeke, 2005).

For the present study the number size distribution of fluorescence biological aerosol particles ($dN_F/d\log D_a$), for each size bin was derived by summing up the particle number concentration from the fluorescence channel numbers 3 – 64 and similarly the total particle number size distribution ($dN_T/d\log D_a$), was derived from channel numbers 1 – 64. In the present study we have used 1.0 μm as a cut-off diameter for given $dN_F/d\log D_a$ and $dN_T/d\log D_a$ to calculate the fluorescence biological aerosol number and total aerosol number concentrations, N_F and N_T, respectively. This is mainly due to the fact that particle counting efficiency of the UV-APS drops below unity at 0.7 μm (counting efficiency ~50% at 0.54 μm) and the interferences from non-biological aerosol particles below 1.0 μm can at times be very high (Huffman et al., 2010). Few other studies have reported a decrease in UV-APS counting efficiency for FBAPs < 2 μm based on comparison of ambient FBAPs with another LIF instrument (WIBS and BioScout) using different fluorescence wavelengths (Healy et al. 2014, Saari et al., 2014). In the present study we define 1 μm as the cutoff diameter to distinguish between the submicron (<1 μm) and the super-micron (>1 μm) modes of the particle number size distribution. The subscripts throughout this manuscript text "F" and "T" refer to fluorescent and total coarse mode particles, respectively. See Table 1 for abbreviations, notations, and symbols used in this manuscript. The particle mass size distributions ($dM/d\log D_a$) for total as well as fluorescent biological aerosol particles were calculated for each size bin by multiplying $dN/d\log D_a$ with volume of an aerodynamically equivalent sphere with the geometric midpoint diameter ($D_{a,g}$) and assuming the unit density (1 g cm^{-3}) and unit shape factor. The integral mass concentrations of coarse fluorescent biological

aerosol particles and total coarse particles, M_F and M_T, respectively were calculated by integrating the particle mass distribution for D_a >1μm, thus particle mass reported here should be viewed as first approximation as a result of uncertainty associated with the density and shape of the particles (Huffman et al., 2010). To be consistent with previous UV-APS results no standard temperature and pressure (STP) corrections were applied to the concentrations reported in this study. These number concentrations can be normalized to the volume that the sampled air would occupy under dry standard condition (STP: 273K, 1000 hPa, and 0% RH) by multiplying the concentration values reported here with a factor of 1.29 derived using ideal gas law.

Fluorescence of sub-micron particles

It has been reported by previous researchers that UV-APS is known to exhibit fluorescence for some fraction of non-biological aerosol particles including soot, PAHs, and cigarette smoke, which could be erroneously counted as FBAP (Huffman et al., 2010; Pan et al., 1999a, 1999b). To investigate the contribution of non-biological aerosol particles that are counted as fluorescence biological aerosol particles, Huffman et al., (2010) showed the correlation between the integrated number concentrations of fluorescent particles (N_F) and total particles (N_T) for different diameter ranges (only for the fluorescence channels >3). To examine the influence of anthropogenic emissions on sub-micron fluorescent particles, we performed a similar correlation analysis for the entire campaign. The correlation between integrated number concentrations of fluorescent particles (N_F) and total particles (N_T) for super-micron (D_a>1μm) and submicron (D_a<1 μm) diameter range exhibited a very poor scatter (R^2=0.03 and R^2=0.002 respectively; N=22280; Figs. S2) indicating extremely small percentage of fluorescence contributed by non-biological aerosol particles in both super-micron and submicron particle ranges. This was in contrast with the observations in Huffman et al (2010).

Since certain component of the mineral dust may exhibit a weak fluorescence (Huffman et al., 2010; Sivaprakasam et al., 2004; Toprak and Schnaiter, 2013), we performed the separate correlation analysis for the *dusty* period, which was dominated by the transport of mineral dust from West Asia, North Africa, and Arabian region (discussed below). The correlation between integrated number concentrations of N_F and N_T for D_a>1 μm was moderately linear (R^2=0.26; N=3138; Fig. S3a) compared to the sub-micron size range during the *dusty* period (R^2=0.007; N=3138; Fig. S3b), indicating that the fraction of super-micron particles exhibiting fluorescence may have been contributed by mineral dust, but not for sub-micron particles.

From these analyses we infer that the contribution of non-biological aerosol particles exhibiting fluorescence was negligible in both sub-micron and super-micron (except during "*dusty* period"; discussed below) size ranges. Thus we hypothesize that due to persistent rainfall the sub-micron and super-micron particles resulting from combustion related activities, were either efficiently removed or were not transported to the observation site. Thus this observation site could be termed as relatively pristine and free from anthropogenic emissions during the monsoon season making this site scientifically interesting for investigating the characteristic properties of bioaerosols on long-term basis using advanced online and offline techniques.

However, to maintain the consistency and uniformity in the comparison of N_F, N_T, and other similar parameters reported in previous studies, all the statistics associated with $dN_F/\mathrm{dlog}\ D_a$ and $dN_T/\mathrm{dlog}\ D_a$ with a cutoff diameter of ~1 μm were derived.

2.4 Meteorological parameter measurement

Meteorological parameters were recorded during the entire campaign using weather sensor (Lufft WS600-UMB) installed on the rooftop at the same height and a few meters away from the UV-

APS inlet (Fig. 1b). These measurements were made concurrently with the UV-APS measurements. The weather station was capable of recording temperature, dew point temperature, relative humidity, precipitation intensity, wind speed, wind direction, and air pressure and was set to record these parameters at 5 minutes interval with time synchronized to UV-APS measurement clock. The meteorological data obtained at this site was compared with data obtained from another weather station (Vaisala WXT520) installed within the close vicinity. The scatter plots between the data (10 minute averages) obtained from both these weather stations exhibited very strong agreement for all the meteorological parameters measured/recorded (average $R^2 \geq 0.95$).

2.5 SEM Analysis

The samples for Scanning Electron Microscopy (SEM) analysis were collected on a 25 mm diameter Nucleopore® Polycarbonate filter paper with pore sizes of 5 µm and 0.2 µm using a two stage filtering method as described by Valsan et al. (2015). All samples were collected for approximate duration of 60 min at an average flow rate of 5 Lpm and were stored in an air-tight container at 4°C until the SEM analysis was carried out. More than 100 individual particles analyzed from samples collected on five occasions during the entire campaign, were investigated using two different scanning electron microscopes – a) Quanta FEG 200 located at the Sophisticated Analytical Instrument Facility (SAIF) and b) Hitachi S 4A00 located at the Chemical Engineering Department of Indian Institute of Technology Madras. Before loading the filter paper on to the sample holders, they were cut into small squares of ~1 cm^2 and sputter coated with gold particles. The biological aerosol particles were identified purely based on their morphological features adopting the method suggested by Matthias-Maser and Jaenicke

(1991,1994). Detailed description on sample collection and analysis was discussed elsewhere (Valsan et al., 2015).

3 Results and discussions

3.1 Campaign overview

Figure 2 shows the temporal evolution and variability of the several meteorological parameters, FBAP, and TAP properties observed throughout the measurement campaign during SW monsoon season at Munnar. Several observations regarding the meteorological conditions during the campaign at Munnar can be made. The predominant wind direction was observed to be Westerly/Southwesterly (Fig. 1), which is characteristic of the monsoon season and bringing nearly clean marine influx (laden with dust and sea salt particles; Vinoj and Satheesh, 2003; Vinoj and Satheesh, 2003; Satheesh and Srinivasan, 2002; Vinoj et al., 2014; Prospero, 1979) over the continent marked by presence of persistent rainfall, high relative humidity (RH), higher wind speeds, and lower temperatures. During this period diurnal variations in temperature and relative humidity were very small and temperatures approached the dew point. On a few occasions, however, Northerly winds were recorded, marked by relatively lower wind speeds, lower RH levels, higher temperatures, and reduced rainfall. During Northerly winds the temperature exhibited more pronounced diurnal variations compared to the relative humidity. The average meteorological parameters (arithmetic mean±standard deviation) recorded during entire measurement period were: (840±1.3) hPa absolute pressure, (17.2±1.4)^{o}C ambient temperature, (96.4±5.7) % relative humidity, (2.8±1.3) m s^{-1} local wind speed, (270)° local wind direction (vector mean weighted by wind speed), and (4188) mm of accumulated rainfall.

The total of more than five months of bioaerosol measurements with high time and size resolution were performed at this site for two contrasting seasons - monsoon (dominated by Southwesterly winds) and winter (dominated by Northeasterly winds). In this study, we present the results from this field campaign carried out during the SW monsoon season whereas the detailed results from the winter campaign from the same measurement site will be presented in a follow up study. We first discuss the characteristic features of the time series as a broad overview of the observed concentration levels, variability, and trends in N_T and N_F. Figure 2 (f,g,h,i,j) shows the time series of geometric mean diameter (D_g, N_F, N_F/N_T, N_T, FBAP and TAP 3-D size distribution measured with the UV-APS for the entire campaign.

Throughout the measurement period the hourly averaged D_g time series consistently remained in the range of ~2 – 4 μm with almost no diurnal variation. During the second half of the campaign, the D_g, however, exhibited relatively high variability with an average mean diameter of 2.6±0.7 μm. Unlike the N_T and N_F the variability in D_g did not seem to be affected by the meteorological parameters except for wind direction (see section 3.4.1) on few occasions. The total coarse particle number concentration, N_T, exhibited high and consistent variability during entire measurement period, however, with no distinct diurnal cycle. Averaged (arithmetic mean±standard deviation) over the entire measurement period was N_T was observed to be 1.8 ± 1.5 cm^{-3} with lowest and highest concentrations of 0.01 cm^{-3} and 8.6 cm^{-3}, respectively. The monthly averaged N_T concentration (Fig. S4) exhibited a decreasing trend from June to August as the monsoon progressed (Tab. 2). In contrast, N_F, exhibited less pronounced but episodic peaks in the time series during the majority of the measurement period, resulting in a campaign arithmetic mean of 0.02 ± 0.02 cm^{-3}. The highest N_F concentration of ~0.52 cm^{-3} was observed in June, prior to the onset of monsoon rainfall, whereas the lowest N_F concentration (<0.0002 cm^{-}

^{3}) was consistently observed on more than one occasion during the months of July and August. The monthly averaged N_F concentrations are listed in Tab. 2.

The time series of relative contribution of FBAP to TAP number, N_F/N_T, exhibited the similar trend in temporal variability as displayed by N_F for most during the campaign. The extreme values of N_F/N_T observed on a few occasions corresponded to low values of N_T implying a negative correlation between N_T and N_F/N_T during these measurements. Huffman et al., (2010) also reported a similar negative correlation between N_T and N_F/N_T at a semi-urban site in central Europe indicating that the variability in N_F/N_T was associated with changes in N_T concentrations. The campaign overview (including individual months) of FBAP mass concentrations and 3-D size distribution for each five minutes of UV-APS measurement are shown in Figure S5.

3.1.1 Particle number and mass concentrations

The number and mass concentration measurements carried out at Munnar over the course of the campaign are shown in Fig. 3 and tabulated in Tab. 2. The box plots show statistical representation of five minute averaged data of the time series. Over the entire measurement period the monthly mean of N_T varied by a factor ~3 from a minimum in August (0.96 cm^{-3}) to a maximum in June (2.7 cm^{-3}; Fig. 3a). The variability of N_T was also found to be highest in the month of June as can be seen from the size of the $5 – 95^{th}$ percentile, which also reflected in the high variability of N_T for entire measurement period. During the initial phase of Southwest monsoon season, the predominant Westerly/Southwesterly winds are known to transport the mineral dust, which constitute large fraction of coarse mode (also in larger diameter size of fine mode fraction) TAP concentration, over the Indian continental region **(**Vinoj et al., 2010, 2014; Li and Ramanathan, 2002; Satheesh and Srinivasan, 2002; Vinoj and Satheesh, 2003). As the monsoon progresses the persistent rainfall can cause the washout of these dust particles along the

path of monsoonal rain, thus reducing the coarse mode TAP concentration (Pranesha and Kamra, 1997a,b; Radke et al., 1980; Moorthy et al., 1991). The monthly arithmetic mean and median average of N_T did not exhibit significant differences. The monthly mean values of N_F varied by the factor of ~4 with moderate variability during the entire campaign (Fig. 3b). Similar to N_T, the monthly mean average value and variability in N_F was highest in the month of June, with mean of 0.03±0.03 cm^{-3} and a 95th percentile value of 0.086 cm^{-3}. The lowest average concentration in N_F (0.007±0.006 cm^{-3}) was observed in the month of July with relatively lower variability as compared to other months of field measurement campaign. Unlike N_T, the arithmetic mean and median average of N_F for individual months exhibited a significant difference as can be seen from the box plot shown in Fig. 3b. The variability of N_F/N_T showed a similar temporal pattern to that displayed by N_F, except that the campaign average mean N_F concentration was higher than that of the August, whereas the campaign averaged mean N_F/N_T was observed to be lower than the mean calculated for August. The median and mean for N_F/N_T, over the course of campaign were ~1 and 2%, respectively (Fig. 3c). The average values of N_F/N_T over this part of the globe were lower than previously investigated sites (Huffman et al., 2010, 2012; Bowers et al., 2009; Schumacher et al., 2013; Matthias-Maser and Jaenicke, 1995; Matthias-Maser et al., 2000; Gabey et al., 2010).

Though, the UV-APS measures particle numbers, the average size-resolved particle mass can also be estimated by assuming the particle density equal to 1 g cm^{-3} (Huffman et al., 2010, 2012). Based on this, the mass concentrations of FBAP (M_F) and TAP (M_T) are presented in Fig. 3. The monthly mean values of M_T exhibited the similar trend and temporal variability as that shown by N_T with overall decrease in M_T as campaign progressed (Fig. 3d). The campaign mean M_T at Munnar was ~7 µg m^{-3}, which was comparable to the values reported from a central European

city (M_T ~7.3 μg m^{-3}) and higher than concentration of M_T (~2.5 μg m^{-3}) reported from a pristine Amazonian rainforest region measured during wet season (Huffman et al., 2010; 2012). The monthly mean values of M_F, on the other hand, did not exhibit a similar pattern to that shown by M_T, but followed a temporal pattern similar to that shown by N_F (Fig. 3e). The highest mean mass concentration of M_F (~0.4 μg m^{-3}) observed during June was ~3 and 2 times lower than the concentrations observed at a central European city (~1.26 μg m^{-3}) and pristine Amazonian rainforest (~0.85 μg m^{-3}), respectively. The higher difference between mean and median values of the box plots indicates the higher temporal variability. The median and mean for M_F/M_T over the course of entire measurement period were 6 and 3% respectively, which is relatively low compared to previously reported studies for various other environments (Huffman et al., 2010; 2012; Artaxo and Hansson, 1995; Schumacher et al., 2013; Fig. 3f). On the average, the relative contribution of FBAP to TAP coarse mode particle mass was ~3 times higher (~6%) than its contribution to coarse mode particle number concentration (~2%). This is consistent with the observations that FBAPs show enhanced prevalence among the larger aerosol particles (Huffman et al., 2010).

3.1.2 Diurnal Patterns

The average diurnal trends for three individual months and the entire measurement campaign were analyzed. Figure 4 shows the mean FBAP values for each hour of the day for three individual months in the campaign, and Fig. S6 shows the corresponding TAP plots. Overall N_F exhibited a moderate diurnal pattern with a consistent early morning (06:00 hr.) peak at ~3 μm (Fig. 4a) except for the month of July, where this early morning peak was absent. A very weak peak during late evening (20:00 hr.) in FBAP concentration at ~3 μm was observed in the month of July. In the month of June, the average diurnal N_F concentration started increasing early in the

evening (~18:00 hr.), which gradually increased through the night reaching maximum at ~06:00 hr. and started decreasing thereafter as the day progressed. A similar diurnal pattern was also observed in August but without high FBAP concentrations in the evening hours. In general, the weak diurnal pattern observed in N_F during the month of July seemed to follow the weak diurnal patterns in RH and temperature, in the presence of persistent rainfall observed during July. The early morning peak at ~3 μm on the diurnal scale was also reported from pristine Amazonian rainforest environment (Huffman et al., 2012). Corresponding average size distributions for entire measurement period will be discussed in details in Sec. 3.3. The diurnal variations of N_T (Fig. S6), on the other hand were very distinct from those of N_F. The size resolved $dN_T/d\log D_a$ for each individual months exhibited a consistent and flat concentration profile at <1 μm. Previous studies where similar instrument was used have reported that pronounced diurnal variations in N_T are strongly coupled with diurnal variations in meteorological variables especially mixing layer depth (Garland et al., 2009; Raatikainen et al., 2014; Du et al., 2013). The absence of pronounced diurnal variations in N_T at this particular site may be a result of weak dependence of coarse mode TAP concentrations on meteorological parameters combined with persistent rainfall causing the washout of these particles (Radke et al., 1980; Raatikainen et al., 2014; Kanawade et al., 2014; Shika et al., 2016). This also indicates the absence of any strong and localized source of anthropogenic emissions during most of the campaign period. Diurnal patterns of N_F/N_T more or less followed the same pattern as that of N_F during all the measurement months. The distinct diurnal pattern in N_F and N_T supports the fact that the sources of TAP and FBAP were different over this region.

The diurnal trends in M_F and M_T for individual months and campaign average were also analyzed and are shown in Figures S7 and S8. The monthly averaged diurnal trends in M_F for individual

months and entire campaign exhibited similar a trend similar to that shown by corresponding to N_F. However, the prominent peak in $dM_F/d\log D_a$ was observed at higher diameter (~3 – 4 μm). The concentration peak of <1 μm observed in N_T shifted to the higher diameter range of ~3 – 4 μm as increase in mass is more associated with presence of coarse mode particles. The distribution of M_T (Fig. S8), however, exhibited a distinctly different trend compared to both M_F and N_T. The distinct diurnal patterns of M_F and M_T showed very less relative contribution of FBAP to TAP mass as compared to other observational sites (Huffman et al., 2010, 2012; Matthias-Maser and Jaenicke, 1995).

3.1.3 Size distribution of particle number and mass

Figure 5 shows the number and mass size distributions for TAPs and FBAPs averaged over the entire measurement period. The TAP number size distribution, $dN_T/d\log D_a$, was generally broad and dominated by a peak at the lower end of the measured size range of number size distribution ($D_a \approx 0.9$ μm; Fig. 5a). In $dN_T/d\log D_a$, the concentrations exhibited a significant decrease above diameter ~3 μm with a long tail extending on the right hand side of the distribution. This peak may be comprised of mineral dust and sea salt particles, as also evident from SEM images (please refer to section 3.3) and as also reported by the previous studies investigating aerosol composition over India during monsoon season (Vinoj et al., 2014; Moorthy et al., 1991; Vinoj and Satheesh, 2003; Satheesh and Srinivasan, 2002; Li and Ramanathan, 2002). A similar peak in $dN_T/d\log D_a$ at $D_a \approx 0.9$ μm was observed in pristine Amazonian rainforest during wet season and was attributed to mineral dust (Huffman et al., 2012; Fig. 5b).The corresponding monthly plots of $dN_T/d\log D_a$ are shown in Fig. S9 and exhibited the similar qualitative number size distribution pattern as that of campaign averaged TAP number size distribution. Averaged over the entire measurement period, the mass size distribution, $dM_T/d\log D_a$ (Fig. 5c), exhibited a

broad peak at ~2.6 μm with an extended tail to the left side of the mass size distribution. The corresponding monthly averaged $dM_T/d\log D_a$ are shown in Fig. S10 and appeared similar to the campaign average TAP mass size distribution. For accurate representation of mass size distribution the unit-normalized mass distribution of D_a plotted in Fig. 5 (c and d) is expected to shift to larger particle size with increased area under the curve (Huffman et al., 2010; DeCarlo et al., 2004).

The campaign average number size distribution of FBAP (Fig. 5b) exhibited monomodal shape with much narrower peak than the TAP number size distribution, with a dominant mode at $D_a \approx 2.8$ μm, which was consistent throughout measurement period. The corresponding monthly mean FBAP number size distributions are shown in Fig. S11. As reported by Huffman et al., (2010) multiple and broader peaks in $dN_F/d\log D_a$ are most likely to originate from different sources and biological species. In the present study, however, we did not find multiple peaks in investigated FBAP number size distribution, suggesting that observed FBAPs comprised the particles from similar or same sources. The overall qualitative appearance of the average FBAP number size distribution is similar to that has been reported by previous measurements. For a semi-urban site in Central Europe Huffman et al., (2010) reported an average FBAP peak at 3.2 μm. Gabey et al., (2010) observed a peak at ~2.5 μm at a tropical rain forest site in Borneo. From a pristine Amazonian rainforest site during wet season Huffman et al., (2012) reported a peak at ~2.3 μm. For another pristine observational site in boreal forest in Finland Schumacher et al., (2013) reported a peak in FBAP number size distribution at ~3 μm. A peak at ~3 μm was also observed by Healy et al., (2014) at a rural site in Killarney national park, Ireland. This dominant peak in the range of 2 – 3 μm in FBAP number size distribution is strongly attributed to the fungal spores over the continent as reported by numerous previous researchers **(**Huffman et al.,

2010, 2012; Schumacher et al., 2013, Li et al., 2011; Artaxo and Hansson, 1995; Healy et al., 2014; Gabey et al., 2010, 2013; Toprak and Schnaiter, 2013**)**. Recently Valsan et al., (2015) investigated the morphological characteristics of PBAPs from the same site during non-monsoon season and found that fungal spores constituted the major fraction of PBAPs and nominally ranged in the size range of ~3 – 10 μm, which roughly translates into equivalent aerodynamic diameter of 2 – 5 μm (assuming particles to be a prolate spheroid) . The scanning electron microscopy images obtained from the filter samples collected during this field campaign showed the strong presence of variety of fungal spore in the size range of 6 – 10 μm (aerodynamic diameter 3 – 5 μm; discussed below; Fig. 11). As an overview of the comparison, the FBAP concentration values observed at Munnar are compared to the FBAP concentration ranges obtained using similar online measurements techniques from diverse environmental conditions across the globe, and the details are tabulated in Tab. 3. The campaign averaged FBAP mass size distribution is shown in Fig. 5d, which nominally appeared bimodal with very sharp primary peak at D_a≈3.2 μm and very broad but small second mode at D_a≈4 μm. The corresponding monthly mean FBAP mass size distributions are shown in Fig. S12. The FBAP mass size distribution for individual months exhibited the similar qualitative shape to that of average campaign.

Figure 6 shows the size-resolved ratio of overall FBAP/TAP for the course of measurement and corresponding monthly ratios are shown in Fig. S13. The relative contribution of FBAPs (dN_F) to TAPs (dN_T) in each size bin could be used to derive the relative contribution of biological particles to total aerosol particles at each size. As reported by Huffman et al., (2010) the assumption of unit density of each particle implies that the value of the dN_F/dN_T ratio would invariably is equal to dM_F/dM_T. The integrated N_F/N_T and M_F/M_T, however, would have the

485 distinct values. As can be seen from Fig. 6 and S13 considerable quantitative and qualitative
486 difference in mean (red) and median (green) curve was consistently observed in all individual
487 months, which likely is the result of poor counting statistics and very high variability in TAP
488 number concentrations. Based on the results presented by Huffman et al., (2010) the mean (red)
489 curve, best represents the N_F/N_T ratios at the upper particle sizes. The mean N_F/N_T ratio curves
490 for individual months and for entire campaign exhibited two dominant peaks persistently in the
491 particle size range ~3 – 4 μm and ~6 – 8 μm. The first prominent peak in dN_F/dN_T distribution at
492 3 – 4 μm comprised 15 – 16% while the second peak at 6 – 8 μm represented ~14 – 15% of the
493 FBAP material in TAP over the entire measurement period (Fig. 6).
494
495 **3.2 Focus periods**
496 The characteristic properties of FBAP and specifically TAP number concentration exhibited
497 strong temporal variability, which could be attributed to changes in prevailing meteorological
498 conditions during monsoon season at Munnar. The following three distinct focus periods during
499 the campaign are highlighted as follows:
500 1. A "*dusty*" focus period was identified when prevailing wind was predominantly
501 Westerly/Southwesterly and air masses mainly came from the Arabian Sea. These were laden
502 with sea salt and dust particles during the start of the monsoon, which dominate the coarse mode
503 fraction of atmospheric aerosols (Vinoj et al., 2014; Li and Ramanathan, 2002) originating from
504 West Asia, North Africa, and Arabian region (Vinoj et al., 2014) and not from local
505 anthropogenic sources. In this campaign, such a dusty period was observed between June 14-25,
506 2014, which was consistent with the description given above and also based on the SEM images
507 of the dust collected in this period (see Sec. 3.5 below). This period was marked with an

accumulated rainfall of ~1015 mm, average relative humidity of 94.4 ± 6.5%, average temperature of 17.7 ± 1.5°C, and average wind speed 2.8±1.3 m s^{-1} (maximum wind speed of 6.7 m s^{-1}).

2. A "*clean*" focus period was observed during latter half of the monsoon season when wind direction was still predominantly Westerly/Southwesterly and air masses originated over Arabian Sea. During this period, which was observed from July 9 – August 7, 2014, FBAP and TAP concentrations were extremely low with very low variability. This *clean* period was associated with persistent rainfall (accumulated rainfall of 2650 mm), average relative humidity of 99.5±1.4%, average temperature of 16.4±0.5°C, and average wind speed 3.7±1 m s^{-1} (maximum wind speed of 8.3 m s^{-1}).

3. A "*high bio*" focus period comprised three discrete events of high FBAP concentration observed between June 1-5, 2014, June 26-30, 2014 and August 18-22, 2014. This period is marked with distinct metrological parameters compared to the *clean* period: accumulated rainfall 194 mm, average relative humidity 93.4±8.4%, average temperature 18.0±2.4°C, and average wind speed 1.2±0.8 m s^{-1} (with maximum wind speed of 4.6 m s^{-1}). It is suggested that these high-bio periods are due to high variability in relative humidity and temperature, and the movement of air masses with relatively low wind speed, over densely vegetated region located north of observational site.

3.2.1 Particle number and mass concentrations

The statistical distributions of N_T, N_F, M_T, M_F, and corresponding ratios for three different focus periods (*dusty*, *clean*, and *high bio*) are shown in Fig. 7 and tabulated in Tab. 4. Each of the focus periods discussed here were not of equal duration. The average total particle number concentration, N_T, showed a decrease of ~70% from *dusty* period to *clean* period (~4.2 cm^{-3} and

~1.3 cm^{-3} respectively), whereas the N_T concentration during *high bio* period was ~1.8 cm^{-3}. The high N_T concentration during the *dusty* period caused the high variability between 5^{th} and 95^{th} percentile in N_T when averaged over entire campaign period (Fig. 3a). The fraction of dust in coarse mode aerosol, which is observed to be very high during pre-monsoon and first few days from the onset of monsoon rainfall, gradually decreased as the monsoon progressed likely as a result of wash out and wet deposition due to persistent rainfall in the path of air masses (Hirst 1953; Madden, 1997; Burge and Roger, 2000). The M_T exhibited similar pattern to that of N_T during three distinct focus periods with average mass concentration of ~16.3 μg m^{-3}, ~5.1μg m^{-3}, and ~7.7 μg m^{-3} for *dusty*, *clean*, and *high bio* periods, respectively (Fig. 7d).

The mean N_F concentration during the *high bio* period (Fig. 7b) was 0.05±0.04 cm^{-3} with high variability in higher concentration range (0.06 – 0.13 cm^{-3}) as evident from the distance between 75^{th} and 95^{th} percentile. The N_F was found to be relatively stable during the *dusty* period with an average concentration of ~0.02±0.008 cm^{-3}. The mean N_F concentration was found to be an order of magnitude lower during the *clean* period (0.005±0.004 cm^{-3}) as compared to *high bio* period, whereas corresponding decrease in N_T from *dusty* to *clean* period (~ by factor of 3) was not of similar magnitude. The following is the hypothesis proposed for such concentration difference in N_F and N_T during the three distinct periods: During the *clean* period the predominant wind direction was Westerly/Southwesterly and air masses came from Arabian Sea bringing clean marine influx marked by persistent rainfall. As a result, the coarse mode aerosol fraction (N_F and N_T) emitted locally were efficiently removed, however, the sea salt particles present in the air masses, which came from Arabian Sea contributed to TAP number concentration (see section 3.3). In addition to the efficient wet removal of FBAP due to persistent rainfall, the high RH level (average 99.5%), causes the dew formation that further inhibit the spore release in turn

554 reducing the FBAP concentration (Schumacher et al., 2013; Jones and Harrison, 2004). The
555 mean values of M_F exhibited trends similar to those shown by N_F, with highest mass
556 concentration of 0.58 μg m^{-3} during *high bio* period, which reduced by ~86% (0.08 μg m^{-3})
557 during the *clean* period. As anticipated the relative contribution of FBAP in TAP during *dusty*
558 and *clean* periods was almost negligible with N_F/ N_T ratio of ~1%. Whereas during the *high bio*
559 period the relative FBAP number and mass contribution to corresponding TAP was ~5% and
560 12% respectively.

561 **3.2.2 Size distribution of particle number and mass concentration**

562 Figure 8a highlights the dN_F/dlog D_a during three distinct focus periods and corresponding
563 dN_T/dlog D_a are shown in Fig. S14. In general dN_F/dlog D_a during each focus period exhibited
564 pattern similar to that of campaign average.

565 The dN_F/dlog D_a averaged over the *high bio* period exhibited a very prominent and sharp peak at
566 ~2.5 – 3 μm. The corresponding dN_F/dlog D_a during *dusty* and *clean* period also exhibited
567 similar bell shaped distribution with less prominent peaks owing to the relatively lower FBAP
568 concentrations as compared to the *high bio* period. Unlike previously reported studies (Huffman
569 et al., 2010; 2012) the peak in dN_F/dlog D_a (D_a≈3 μm) was not reflected in dN_T/dlog D_a mostly
570 due to relatively less contribution of FBAP in coarse mode TAP number concentration. As seen
571 from Fig. S14 the total aerosol particle number size distribution, dN_T/dlog D_a, during all the three
572 focus periods exhibited almost similar pattern to that of campaign averaged dN_T/dlog D_a with
573 higher concentrations peaking at lower diameter.

574 The FBAP mass size distribution (Fig. 8b) during *dusty* period was dominated by bimodal peaks
575 with prominent peak at ~3 μm and a relatively less pronounced peak in the range of ~4 – 6 μm
576 showing broader tail on the right side of the distribution curve. The dM_F/dlog D_a, during *clean*

period, exhibited similar bimodal peaks with extended shoulder in the diameter range from ~4 to 7 μm. The $dM_F/d\log D_a$ distribution during *high bio* period was distinctly different compared to the two other focus periods discussed above with a prominent monomodal peak at ~3 μm. The primary peak observed in $dM_F/d\log D_a$ in the range of ~3 to 4 μm was consistent during individual months and different focus periods. TAP mass size distribution (Fig. S15) exhibited similar qualitative pattern to that of campaign averaged $dM_T/d\log D_a$ with peak between ~2.5 to 3.5 μm with an extended tail on the right side, which gradually increased for D_a>13 μm. The statistics representing 5th, 25th, 75th, and 95th percentile for $dN_F/d\log D_a$ and $dM_F/d\log D_a$ during individual focus periods are shown in Fig. S16 and S17.

The size resolved ratio of FBAP to TAP particles averaged for three distinct focus periods is shown in Fig. 9. As evident from the figure the largest fraction of FBAP particles during *dusty* period occurred between ~ 6 – 9 μm (~20%) with relatively small (~7%) contribution in the diameter range of ~ 3 – 4 μm. The fact that N_F/N_T is near zero for particle size below ~1.5 μm is in line with previous observations reported from a semi urban site in central Europe and during wet season of pristine Amazonian rainforest (Huffman et al., 2010; 2012). During the *clean* period the maximum contribution of FBAP to TAP number concentration reduced to ~10.5% in the diameter range of ~ 6 to 9 μm, but the peak appeared at ~3 – 4 μm and remained almost consistent with relative contribution of ~8%. Whereas during *high bio* period the maximum contribution of FBAP to TAP occurred between broader size range of ~ 3 – 8 μm with contribution range of ~28 – 19%. Interestingly during the *high bio* period, the highest contribution of FBAP to TAP number concentration occurred at $D_a \approx 3.5$ μm, as opposed to the other two focus periods when the highest contribution was observed in the larger diameter ranges of ~ 6 – 8 μm. N_F/N_T was consistently found to be very low, with values approaching zero for the

diameter beyond 13 μm, indicating FBAP constituted an extremely small fraction of total aerosol particles (Huffman et al., 2010; 2012). The two prominent peaks observed during the focus periods were clearly evident in campaign-averaged dN_F/dN_T (Fig. 6; peaks at ~3.5 and 6 μm).

3.2.3 Diurnal patterns

A prominent early morning peak in N_F during the *high bio* period in the diameter range of 1.5 – 3 μm was observed from 06:00 to 08:00 hrs., which clearly reflected in campaign averaged diurnal patterns at the same hour of the day. The diurnal variations in N_F during the *dusty* and *clean* periods were not so pronounced (Fig. 10) as compared to the variations during the *high bio* period. During the *dusty* period, N_F showed slightly high concentration starting from ~17:00 hrs. (lowest panel Fig. 10a) and persistently remained high until early morning without any variations, whereas during the *clean* period, N_F concentration consistently remained flat throughout 24 hours. As reported by Huffman et al., (2012) the emission and dispersal of bioaerosols is strongly coupled with environmental variables such as solar radiation, temperature, and relative humidity. Each of these variables exhibited relatively pronounced diurnal variations during the *high bio* period (upper panel Fig. 10c). It has been well documented that relative humidity, in particular, plays an important role in active wet discharge of fungal spores (Adhikari et al., 2006; Burch and Levetin, 2002; Elbert et al., 2007; Jones and Harrison, 2004; Quintero et al., 2010; Zhang et al., 2010) , which constitutes major fraction of atmospheric bioaerosols (Ansari et al., 2015; Bauer et al., 2008; Bowers et al., 2013; Fröhlich-Nowoisky et al., 2009; Sesartic and Dallafior, 2011; Spracklen and Heald, 2014). The meteorological parameters exhibited significant diurnal variations during the *high bio* period, where RH decreased to a level ~60 – 80%, which is considered to be favorable for release of the fungal spores (Jones and Harrison, 2004; Santarpia et al., 2013). During the *dusty* and *clean* periods, the

623 persistence of high RH values in the range of ~90 – 100%, might have inhibited the active wet
624 discharge of fungal spore (Schumacher et al., 2013) thus resulting in the weak diurnal variation
625 in N_F. Unlike N_F, N_T remained nearly flat without any pronounced diurnal variations during three
626 distinct focus periods (Fig. S18). The corresponding diurnal cycle of FBAP mass concentration
627 and 3D size distributions for three focus periods are shown in Fig. S19. M_F exhibited similar
628 diurnal patterns to that of N_F during three distinct focus periods. M_T and N_T remained flat during
629 the *dusty* period, but exhibited slightly pronounced diurnal pattern during the *clean* and the *high*
630 *bio* period between 09:00 hrs. and 16:00 hrs. (Fig. S20).
631
632 **3.3 SEM images**
633 Figure 11 shows representative SEM images of different biological particle types often observed
634 during the SW monsoon season at Munnar. The details about the sampling techniques,
635 instrument used, etc. for obtaining these bioaerosol images are discussed in details by Valsan et
636 al., (2015). Note that these images are being presented here to showcase the particle types
637 consistently observed throughout the measurement period and not for quantitative purposes. The
638 presence of mineral dust and sea salt particles confirms marine influence of the air mass
639 sampled. Many particles observed by SEM were most likely Basidiospores. The appearance of
640 small protuberances on their surfaces suggests that the spores (e.g. Fig. 11a and c) most likely
641 belonged to the *Hydnaceae* family (Grand and Vandyke, 1976; Valsan et al., 2015). The
642 Basidiospores shown in Fig. 11b and c were seen in abundance in all the samples collected
643 during the campaign. Some of the spores observed appeared to be coated with salt particles (Fig
644 11e) and might have been carried from a distant source by the SW monsoon winds. The spores
645 shown in Fig 11 (d and f) most likely appeared to be spores of Ascomycota division. The particle

shown in Fig. 11g was most likely a mineral dust particle sampled during high dusty episode. Similar particles of varying size during the *dusty* episode were consistently observed during SEM analysis. Fig 11h and 11i shows the images of the typical sea salt particles observed during samples collected at Munnar during measurement campaign when wind predominantly came from Westerly/Southwesterly direction travelling over Indian Ocean and Arabian Sea.

3.4 Meteorological Correlations

The results obtained with UV-APS data analysis during the campaign at Munnar were correlated with meteorological parameters to investigate factors responsible for bioaerosol release and their variations in the atmosphere.

3.4.1 Impact of wind direction

The wind rose diagrams scaled by N_F, D_g, and $D_{g,T}$ were also prepared for entire measurement period and three distinct focus periods. These plots are similar to the traditional wind rose diagram (Fig. S21) except that, instead of wind speed, they are scaled by characteristic FBAP and TAP parameters, which indicate the frequency of occurrence of respective parameter with respect to wind direction (Sherman et al., 2015). As seen from Fig. S21, predominant wind direction during entire campaign was Westerly/Southwesterly with frequency of occurrence of about ~90%. The wind speed broadly ranged between 2 – 5 m s^{-1} with no prominent diurnal variations. The overall wind direction and back trajectory analysis (Fig. 1) shows that the sampled air masses may have originated over the Indian Ocean and then turning eastward after crossing the equator and travelling several hundred kilometers over Arabian Sea before reaching the observational site (Fig. 1). The predominant wind pattern during the *dusty* (>95% frequency of occurrence; 2 – 6 m s^{-1}) and *clean* periods (~100 frequency of occurrence; 2 – 6 m s^{-1}) was

669 Westerly/Southwesterly. Whereas during the *high bio* period only ~50% of the time winds came
670 from Westerly/Southwesterly direction and rest comprised of relatively slower (0 – 2 m s^{-1})
671 winds from all other directions with highest contribution of northerly winds (Fig. S21).
672 Wind rose diagram scaled by FBAP number concentration is shown in Fig. 12. During the entire
673 campaign the predominant wind showed that ~85% of the time FBAP concentration occurred in
674 the range of 0 – 0.05 cm^{-3} (Fig. 12a) occasionally exceeding 0.05 cm^{-3} and was contributed by
675 Westerly/Southwesterly winds. The occurrence of relatively low FBAP concentration during
676 entire campaign is coincidental with low concentration occurrence during the *dusty* (0 – 0.05
677 cm^3; >90% frequency of occurrence) and the *clean* (<0.01 cm^3; ~90% frequency of occurrence)
678 periods. During the *high bio* period the FBAP concentration, >0.05 cm^3 exhibited ~40%
679 frequency of occurrence of which ~50% was contributed by predominant wind from the North
680 and the Northwest.
681 Similarly the wind rose diagram scaled by geometric mean diameter (D_g) of $dN_F/d\log D_a$, is
682 shown in Fig. 13. The average size of the FBAP particles associated with
683 Westerly/Southwesterly winds when analyzed for the entire campaign ranged between 2 – 4 μm
684 of which ~65% of the time D_g was observed to be ≤3 μm. During the three focus periods the
685 frequency of occurrence of FBAP particles in the higher size range (3 – 4 μm) was strongly
686 associated with the Westerly/Southwesterly winds (Figs. 13b – d). The corresponding wind rose
687 diagram scaled by geometric mean diameter of $dN_T/d\log D_a$ ($D_{g,T}$) is shown in Fig. S22. During
688 entire measurement campaign the frequency of occurrence of $D_{g,T}$ in the size range of 0.8 – 0.9
689 μm was ~70% and was mostly associated with Westerly/Southwesterly winds. During the *dusty*
690 period, particles in the size range of 0.8 – 0.9 μm diameter contributed for >95% frequency of
691 occurrence for the entire size range, whereas during *clean* period ~20% occurrence of the

692 particles in the size range other than 0.8 – 0.9 μm were also observed. On the other hand during
693 the *high bio* period total particles in the size range 0.5 – 0.8 μm were observed with ~50%
694 frequency of occurrence mostly dominated by northerly winds.
695 The FBAP concentration exhibited strong dependence on the wind direction for this
696 observational site. During the *high bio* period the increase in frequency of occurrence of FBAP
697 number concentrations >0.1 cm^{-3} coincided with lower wind speed coming from the North and
698 Northwest (Fig. 14a). During the *high bio* period, as in the case of the *dusty* and *clean* periods,
699 the predominant wind pattern was Westerly/Southwesterly, but, with relatively low frequency of
700 occurrence as compared to the other two periods. To have a better understanding of the relative
701 contribution of wind direction in high FBAP number concentration during the *high bio* period,
702 separate wind rose diagrams for FBAP concentration >0.1 cm^{-3} and <0.1 cm^{-3} as shown in Fig.
703 14. The FBAP number concentration >0.1 cm^{-3} was associated with lower wind speed (0 – 1 m s^{-1};
704 ~80% frequency of occurrence) and predominant Northerly winds (Fig. 14a) as opposed to
705 high wind speed (2 – 5 m s^{-1}) and predominant Westerly/Southwesterly winds for the FBAP
706 number concentration <0.1 cm^{-3} (Fig. 14b). The Northerly winds with lower wind speed coming
707 over from densely vegetated regions in combination with local FBAP sources during the *high bio*
708 period could be the strong reason for the build up resulting in higher FBAP number
709 concentration during this episode, whereas, Westerly/Southwesterly winds were consistently
710 marked by very low FBAP number concentration mostly owing to higher wind speeds. Further, it
711 might also due to the fact that the air masses arriving at observational site originating over
712 cleaner marine region, which may be potential but weak source of bioaerosols combined with
713 possible wash out/wet deposition due to persistent rainfall during the transport. The frequency of
714 occurrence of larger particles (3 – 4 μm) during Westerly/Southwesterly winds was high

compared to the Northerly winds, where particles were mostly of smaller size (1 – 3 μm). We hypothesize that during the Northerly wind the bioaerosols were mostly comprised of Basidiospores, which is consistent with SEM images obtained during measurement period. Frohlich-Nowoisky et al., (2012) reported that, a region with dominant prevalence of marine air masses has larger proportions of Ascospores and in contrast, the continental air masses exhibit higher proportions of Basidiosppres. However, due to technical difficulties associated with sampling we could not establish the identity of the spores observed at this observational site during Westerly/Southwesterly winds and these details will be addressed in follow up studies. The corresponding wind rose scaled by $D_{g,T}$ obtained from $dN_T/d\log D_a$ is shown in Fig. S23.

As shown in Tab. 5 the wind speed was observed to correlate negatively with N_F during entire measurement period and is consistent with previously reported studies (Hameed et al., 2012; Almaguer et al., 2013; Lyon et al., 1984; Quintero et al., 2010). The increased N_F concentration levels during lower wind speed might indicate that observed bioaerosols were dominated by the local source rather than transported from longer distances (Sadys et al., 2014; Hara and Zhang, 2012; Bovallius et al., 1978; Maki et al., 2013; Prospero et al., 2005; Creamean et al., 2013) as lower wind speed may actually increase emission of some specific type of spores (Huffman et al., 2012; Jones and Harrison, 2004; Troutt and Levetin, 2001; Kurkela, 1997).

3.4.2 Correlation with relative humidity and temperature

Correlation coefficient derived between N_F and relative humidity averaged over the entire campaign is shown in Fig. 15 and corresponding R^2 values for three distinct focus periods are shown in Tab. 5. In general an increase in N_F concentration with increasing relative humidity was observed with moderate correlation coefficient (R^2=0.58). Depending upon the type of bioaerosols, geographical location, and local climate, N_F has shown varied dependence on

738 relative humidity and the precise response of the spore concentration to relative humidity is
739 difficult to characterize. For example, a number of studies have shown that spores of genus like
740 *Cladosporium*, *Alternaria*, and *Epiccocum* are known to exhibit the negative correlation with
741 relative humidity (Oliveira et al., 2010; Herrero et al., 1996; Kurkela, 1997; Oh et al., 1998;
742 Healy et al., 2014); while on the other hand, other studies have also found these spores to be
743 positively correlated with relative humidity (Quintero et al., 2010; Hjelmroos, 1993; Ho et al.,
744 2005). Genus like *Ustilago* and some other Basidiospores may exhibit strong positive correlation
745 with relative humidity (Sabariego et al., 2000; Quintero et al., 2010; Ho et al., 2005; Calderon et
746 al., 1995). Ascospores concentrations are known to increase during and after rainfall (Burch and
747 Levetin, 2002; Elbert et al., 2007; Hasnain, 1993; Hirst, 1953; Toutt and Levetin, 2001; Lyon et
748 al., 1984; Oh et al., 1998) whereas Basidiospores exhibited a strong resemblance to the diurnal
749 pattern of relative humidity (Li and Kendrick 1994; Hasnain 1993; Tarlo et al., 1979; Trout and
750 Levetin 2001). Almaguer et al., (2013) have reported that in a tropical region, relative humidity
751 has greater influence than temperature on the airborne spore counts and may be a pre-requisite
752 for release of spores (Hollins et al., 2004). Thus, the combination of persistent threshold relative
753 humidity (~60 – 95% as reported by Ho et al., 2005) and rainfall can cause the increase in the
754 spore concentration and the excessive and persistent rain, however, tends to wash the spore out
755 of the atmosphere further reducing their concentration levels (Burge 1986; Horner et al., 1992;
756 Troutt and Levetin, 2001). Based on these arguments combined with observed meteorological
757 conditions we expect that the bioaerosols reported here from Munnar mainly consisted of
758 Basidiospores during the SW monsoon season as also evident from SEM images (discussed
759 above). This is consistent with results reported by Valsan et al., (2015) where they found the
760 dominant presence of dry air spora (*Cladosporium*) during relatively dry and warm weather from

the same observational site. In general, N_F and N_F/N_T decreased with increasing wind speed (R^2=0.6 and R^2=0.78, respectively) indicating that wind speed may be one of the strong factors for observed high N_F concentrations at this site. As compared to previously reported correlation between N_F and meteorological parameters (Santarpia et al., 2013), the relations shown for this observational site appeared to be more robust and conclusive. The variability observed in N_T (N_T - $N_{T,min}$/ $N_{T,max}$- $N_{T,min}$; not shown here) was more consistent and high as compared to variability observed in N_F (N_F – $N_{F,min}$/ $N_{F,max}$- $N_{F,min}$), which was more episodic and hence one would expect the weak correlation between N_T and meteorological parameters (Tab. 5).

Several studies have reported that in temperate regions, temperature is probably the most important meteorological parameter affecting the spore concentration (Levetin and Horner, 2002; Adhikari et al., 2006) with highest spore concentration during summer season (Emberlin et al., 1995; Hasnain, 1993; Herrero et al., 1996; Hjelmroos, 1993; Li et al., 2011; Schumacher et al., 2013). When the relation between temperature and spore concentration was investigated on the basis of diurnal average, spore concentration have been observed to decrease with the increasing temperature (Burch and Levetin, 2002; Calderon et al., 1995; Sabariego et al., 2000; Schumacher et al., 2013; Trejo et al., 2013). Consistent with this trend, we have found significant negative correlation between N_F and temperature (R^2=0.65) averaged over the entire measurement period at Munnar. The correlation coefficient between N_F and temperature for three distinct focus periods is given in Tab. 5 and are specific to this locality of sampling and may not be extrapolated to represent behavior in other ecosystems in the Indian region. These results were, however, presented to formulate preliminary hypothesis about role of meteorological parameters in governing the variability of bioaerosols specific to this observational site for the monsoon season.

4 Summary and Conclusions

A UV-APS was continuously operated during the SW monsoon season (June 1 - August 21, 2014) at Munnar in the Western Ghats in Southern tropical India. The number and mass size distributions and corresponding concentrations of biological aerosol were quantified for three distinct focus periods namely *dusty*, *high-bio*, and *clean*, identified based on the prominent wind direction. Over the course of the entire measurement period the coarse particle number concentration of FBAPs varied in the range of 0.2×10^{-3} cm^{-3} to 0.63 cm^{-3} with an arithmetic mean value of 0.02 cm^{-3} (±0.02 cm^{-3}). This average concentration accounted for 0.04 – 53% (mean value 2.1%±4.05%) of the total coarse particle number concentration. The coarse particle mass concentrations of FBAPs varied in the range of 0.5×10^{-3} – 4.93 μg m^{-3} with an arithmetic mean (±standard deviation) value of 0.24 (±0.28) μg m^{-3}.

The FBAP concentrations observed at Munnar during SW monsoon season were within the range but slightly on the lower side of the concentrations reported by previous researchers using various online and offline techniques from varying environments (Despres et al., 2007; Huffman et al., 2010, 2012; Adhikari et al., 2004; Bovallius et al., 1978; Bowers, et al., 2009, 2013; Lee et al., 2010; Matthias-Maser and Jaenicke, 1995; Matthias-Maser et al., 2000; Shaffer and Lighthart, 1997; Tong and Lighthart, 1999; Wang et al., 2007; Li et al., 2011; Hameed et al., 2009; Bauer et al., 2008; Schumacher et al., 2013; Gabey et al., 2010, 2011, 2013; Saari et al., 2015; Toprak and Schnaiter, 2013; Healy et al., 2014). For brevity, here we compare the number concentrations observed at Munnar only with number concentrations from varying environments carried out using online measurements. Huffman et al., (2010) have reported coarse mode average FBAP number concentration from four months of measurement to be 0.03 cm^{-3}, which

constituted ~4% of total coarse mode particles from a semi-urban site of Mainz in Central Europe. The median FBAP concentration during the wet season of pristine tropical Amazonian rainforest region was found be 0.07 cm^{-3}, which constituted ~24% of total coarse mode particle number concentration (Huffman et al., 2012). By analyzing the full one-year observations from Boreal forest in Hyytiala and pine forest in Colorado, Schumacher et al., (2013) reported highest FBAP concentration in summer of 0.046 cm^{-3} (constituting ~13% of total coarse mode particles) and 0.03 cm^{-3} (constituting ~8.8% of total coarse mode particles), respectively. Healy et al., (2014) reported the average FBAP concentration of ~0.01 cm^{-3} using the UV-APS measurements carried out with in the Killarney national park, Kerry situated in Southwest of Ireland. Gabey et al., (2013) by performing the measurements at a high altitude site in central France reported averaged FBAP concentration of 0.012 cm^{-3} and 0.095 cm^{-3} using two-wavelength (280 nm and 370 nm respectively) single-particle UV-induced fluorescence spectrometer. Gabey et al., (2010) from tropical rainforest in Borneo, Malaysia reported that mean FBAP number fraction in the size range of 0.8 – 20 μm was ~55% and ~28% below and above the forest canopy, respectively. It is important to note, however, that the measurement results compared here were obtained from different instrumentation operating with different wavelength.

The average observed $dN_F/d\log D_a$ exhibited a peak at ~3 μm, which was consistent even during distinct focus periods with slight quantitative variation in the FBAP number concentration. Such a consistency in the peak of $dN_F/d\log D_a$ during entire measurement period indicates that sources and type of bioaerosols did not exhibit considerable variability and diversity at Munnar during SW monsoon season. The peak observed in $dN_F/d\log D_a$ in this study is consistent with range of the peaks published by previous researchers. At a semi-urban site in Central Europe the peak in $dN_F/d\log D_a$ was observed at ~3 μm (Huffman et al., 2010). In pristine tropical rainforest region

of Amazonia a peak in $dN_F/d\log D_a$ was found at ~2.5 μm (Huffman et al., 2012). Whereas the peak in $dN_F/d\log D_a$ at a boreal forest in Finland exhibited a strong seasonal dependence with different modes at ~1.5 μm, ~3 μm, and ~5 μm indicating differences in the bioaerosol sources (Schumacher et al., 2013). In the pine forest of Colorado the distinct peaks were observed at ~1.5 μm and ~5 μm (Schumacher et al., 2013). The mode at ~3 μm reported for Colorado is likely due to the fungal spore whose release mechanism is strongly governed by the combination of relative humidity and temperature (Huffman et al., 2010 and references therein).

On the diurnal scale a pronounced diurnal cycle with ~3 μm peak with a maximum concentration at ~06:00 hr. was observed when averaged over entire measurement period. This general pattern is consistent with previous studies reporting the early morning peak in FBAP concentration for various environmental conditions (Healy et al., 2014; Huffman et al., 2012; Schumacher et al., 2013; Toprak and Schnaiter, 2013). The early morning peak was contributed by Basidiospores as their release in the atmosphere is strongly coupled with relative humidity (Adhikari et al., 2006; Burch and Levetin, 2002; Hasnain, 1993; Healy et al., 2014; Ho et al., 2005; Huffman et al., 2012). This is also consistent with the SEM images shown and discussed above.

The meteorological parameters were observed to correlate significantly with FBAP concentration at Munnar. We observed that N_F followed the similar diurnal trend to that of relative humidity and was anti-correlated with temperature. As reported by previous studies from selected locations (Huffman et al., 2013; Schumacher et al., 2013; Prenni et al., 2013; Hirst 1953) we did not observe any sharp increase in N_F concentration immediately after or during rainfall. We hypothesize that the spore built-up and release of certain species can happen only at certain threshold relative humidity (Jones and Harrison, 2004). Our results indicate that under the dry environmental conditions where relative humidity levels rarely attain such threshold required for

fungal spore release can cause the strong built up of fungal spores inside fungal bodies. Under these conditions precipitation can cause the relative humidity levels to increase up to threshold required for fungal spore release in combination with mechanical splashing due to raindrops, and can cause the sudden and sharp increase in spore concentrations. On the contrary, like in present case, the persistent high humidity conditions can cause the continuous release of the spore without an opportunity for built-up of fungal spores in fungal body to be released during rainfall. It is also reported that persistent high levels of relative humidity can inhibit the sporulation (Schumacher et al., 2013) further considerably reducing the spore release. More detailed measurements are required from the regions where relative humidity persistently remains low (<60%) for extended amount of time and experiences sudden rainfall. The correlation between N_F and wind speed was found to be strongly negative. Since majority of the spore release was dominated by the local sources, the strong winds coming over from West/Southwest direction, which were relatively clean, might have caused the dilution of air mass thus reducing the spore concentration.

Overall, the long-term measurements reported in this manuscript showed the quantitative and qualitative agreement with previously reported studies. The emissions and abundance of biological aerosol particles in Western Ghats air during monsoon season appeared to be closely linked to the variability in the meteorological parameters. The scatter plot analysis carried out between N_F and N_T for submicron and super-micron particles indicated that submicron particles at this observational site were also dominated by aerosol particles of biological origin, thus indicating the lowest possible interference from particles of anthropogenic origin known to exhibit the fluorescence at the prescribed wavelength used in UV-APS. Hence, given observational site can be termed as relatively pristine while under the influence of SW monsoon

season. This emphasizes the need to perform similar measurements under different land-use type during same season over Indian region. The contrasting characteristics of this observational site associated with pollution and interference of non-biological aerosol particles in fluorescence will be discussed in follow up studies. We propose more studies by means of performing simultaneous online measurements of biological aerosol particle under contrasting environments during distinct meteorological seasons over Indian region. These measurements could be supplemented with advanced offline measurement techniques including SEM analysis, DNA analysis, and fluorescence microscopy of the samples collected in parallel with the measurements. We believe that such a comprehensive approach over Indian region would be helpful in understanding the possible tight coupling between aerosol and hydrological cycle especially during monsoon. This could also help to better understand the implication of biological aerosols on crops and human health where agricultural industry has the major share in GDP to cater the need of 18% of the world's total population.

Acknowledgement:

SSG acknowledge the combined financial support from Max Planck Society and Department of Science and Technology, Government of India under the Max Planck Partner Group Program. Authors are thankful to Akila M, Hema P, Shika S, Aliena, Hasitha, Reshma, Sanu, and Tabish U. Ansari for their support in planning, execution, and completion of the measurement campaign. Authors thankfully acknowledge the support from Gerhard Lammel, Multiphase Chemistry Department, Max Planck Institute for Chemistry for his support during campaign and providing the meteorological data for comparison. Authors are grateful to the Sophisticated Analytical Instrument Facility (SAIF), IIT Madras for making SEM available for morphological analysis. Authors gratefully acknowledge US Geological Survey for the topography data in DEM format and NOAA ARL for providing HYSPLIT air mass back trajectory calculations.

References:

Adhikari, A., Sen, M. M., Gupta-Bhattacharya, S., and Chanda, S.: Air-borne viable, non-viable, and allergenic fungi in a rural agricultural area of India: a 2-year study at five outdoor sampling stations, Science of the Total Environment, 326, 123-141, 10.1016/j.scitotenv.2003.12.007, 2004.

Adhikari, A., Reponen, T., Grinshpun, S. A., Martuzevicius, D., and LeMasters, G.: Correlation of ambient inhalable bioaerosols with particulate matter and ozone: A two-year study, Environmental Pollution, 140, 16-28, 10.1016/j.envpol.2005.07.004, 2006.

Agranovski, V., Ristovski, Z., Hargreaves, M., Blackall, P. J., and Morawska, L.: Performance evaluation of the UVAPS: influence of physiological age of airborne bacteria and bacterial stress, Journal of Aerosol Science, 34, 1711-1727, 10.1016/s0021-8502(03)00191-5, 2003.

Agranovski, V., Ristovski, Z. D., Ayoko, G. A., and Morawska, L.: Performance evaluation of the UVAPS in measuring biological aerosols: Fluorescence spectra from NAD(P)H coenzymes and riboflavin, Aerosol Sci. Technol., 38, 354-364, 10.1080/02786820490437505, 2004.

Agranovski, V., and Ristovski, Z. D.: Real-time monitoring of viable bioaerosols: capability of the UVAPS to predict the amount of individual microorganisms in aerosol particles, Journal of Aerosol Science, 36, 665-676, 10.1016/j.jaerosci.2004.12.005, 2005.

Almaguer, M., Aira, M.-J., Rodríguez-Rajo, F. J., and Rojas, T. I.: Temporal dynamics of airborne fungi in Havana (Cuba) during dry and rainy seasons: influence of meteorological parameters, International Journal of Biometeorology, 58, 1459-1470, 10.1007/s00484-013-0748-6, 2013.

Andreae, M. O., and Rosenfeld, D.: Aerosol-cloud-precipitation interactions. Part 1. The nature and sources of cloud-active aerosols, Earth Science Reviews, 89, 13-41, 2008.

Ansari, T. U., Valsan, A. E., Ojha, N., Ravikrishna, R., Narasimhan, B., and Gunthe, S. S.: Model simulations of fungal spore distribution over the Indian region, Atmospheric Environment, 122, 552-560, http://dx.doi.org/10.1016/j.atmosenv.2015.10.020, 2015.

Artaxo, P., and Hansson, H. C.: Size distribution of biogenic aerosol-particles from the Amazon basin, Atmospheric Environment, 29, 393-402, 10.1016/1352-2310(94)00178-n, 1995.

Baron, P. A., and Willeke, K.: Aerosol Measurement – Principles, Techniques and Applications, Second edition, John Wiley & Sons. 2005.

Bauer, H., Schueller, E., Weinke, G., Berger, A., Hitzenberger, R., Marr, I. L., and Puxbaum, H.: Significant contributions of fungal spores to the organic carbon and to the aerosol mass balance of the urban atmospheric aerosol, Atmospheric Environment, 42, 5542-5549, 10.1016/j.atmosenv.2008.03.019, 2008.

Bhati, H. S., and Gaur, R. D.: Studies on Aerobiology - Atmospheric fungal spores, New Phytologist, 82, 519-527, 10.1111/j.1469-8137.1979.tb02678.x, 1979.

Bovallius, A., Bucht, B., Roffey, R., and Anas, P.: 3-Year investigation of natural airborne bacterial-flora at 4 localities in Sweden, Applied and Environmental Microbiology, 35, 847-852, 1978.

Bowers, R. M., Lauber, C. L., Wiedinmyer, C., Hamady, M., Hallar, A. G., Fall, R., Knight, R., and Fierer, N.: Characterization of Airborne Microbial Communities at a High-Elevation Site

940 and Their Potential To Act as Atmospheric Ice Nuclei, Applied and Environmental
941 Microbiology, 75, 5121-5130, 10.1128/aem.00447-09, 2009.

942 Bowers, R. M., Clements, N., Emerson, J. B., Wiedinmyer, C., Hannigan, M. P., and Fierer, N.:
943 Seasonal Variability in Bacterial and Fungal Diversity of the Near-Surface Atmosphere,
944 Environmental Science & Technology, 47, 12097-12106, 10.1021/es402970s, 2013.

945 Brosseau, L. M., Vesley, D., Rice, N., Goodell, K., Nellis, M., and Hairston, P.: Differences in
946 detected fluorescence among several bacterial species measured with a direct-reading particle
947 sizer and fluorescence detector, Aerosol Sci. Technol., 32, 545-558, 10.1080/027868200303461,
948 2000.

949 Burch, M., and Levetin, E.: Effects of meteorological conditions on spore plumes, International
950 Journal of Biometeorology, 46, 107-117, 10.1007/s00484-002-0127-1, 2002.

951 Burge, H. A.: Some comments on the aerobiology of fungus spores, Grana, 25, 143-146, 1986.

952 Burge, H. A., and Rogers, C. A.: Outdoor allergens, Environmental Health Perspectives, 108,
953 653-659, 10.2307/3454401, 2000.

954 Burrows, S. M., Butler, T., Jöckel, P., Tost, H., Kerkweg, A., Pöschl, U., and Lawrence, M. G.:
955 Bacteria in the global atmosphere - Part 2: Modeling of emissions and transport between
956 different ecosystems, Atmos. Chem. Phys., 9, 9281-9297, 2009.

957 Calderon, C., Lacey, J., McCartney, H. A., and Rosas, I.: Seasonal and diurnal-variation of
958 airborne basidiomycete spore concentrations in Mexico-city, Grana, 34, 260-268, 1995.

959 Chakraborty, P., Gupta-Bhattacharya, S., Chakraborty, C., Lacey, J., and Chanda, S.: Airborne
960 allergenic pollen grains on a farm in West Bengal, India, Grana, 37, 53-57, 1998.

961 Coz, E., Artinano, B., Clark, L. M., Hernandez, M., Robinson, A. L., Casuccio, G. S., Lersch, T.
962 L., and Pandis, S. N.: Characterization of fine primary biogenic organic aerosol in an urban area
963 in the northeastern United States, Atmospheric Environment, 44, 3952-3962,
964 10.1016/j.atmosenv.2010.07.007, 2010.

965 Creamean, J. M., Suski, K. J., Rosenfeld, D., Cazorla, A., DeMott, P. J., Sullivan, R. C., White,
966 A. B., Ralph, F. M., Minnis, P., Comstock, J. M., Tomlinson, J. M., and Prather, K. A.: Dust and
967 Biological Aerosols from the Sahara and Asia Influence Precipitation in the Western U.S,
968 Science, 339, 1572-1578, 10.1126/science.1227279, 2013.

969 DeCarlo, P. F., Slowik, J. G., Worsnop, D. R., Davidovits, P., and Jimenez, J. L.: Particle
970 morphology and density characterization by combined mobility and aerodynamic diameter
971 measurements. Part 1: Theory, Aerosol Sci. Technol., 38, 1185-1205, 2004.

972 DeLeon-Rodriguez, N., Lathem, T. L., Rodriguez-R, L. M., Barazesh, J. M., Anderson, B. E.,
973 Beyersdorf, A. J., Ziemba, L. D., Bergin, M., Nenes, A., and Konstantinidis, K. T.: Microbiome
974 of the upper troposphere: Species composition and prevalence, effects of tropical storms, and

atmospheric implications, Proceedings of the National Academy of Sciences of the United States of America, 110, 2575-2580, 10.1073/pnas.1212089110, 2013.

Despres, V. R., Nowoisky, J. F., Klose, M., Conrad, R., Andreae, M. O., and Poschl, U.: Characterization of primary biogenic aerosol particles in urban, rural, and high-alpine air by DNA sequence and restriction fragment analysis of ribosomal RNA genes, Biogeosciences, 4, 1127-1141, 2007.

Despres, V. R., Huffman, J. A., Burrows, S. M., Hoose, C., Safatov, A. S., Buryak, G., Frohlich-Nowoisky, J., Elbert, W., Andreae, M. O., Poschl, U., and Jaenicke, R.: Primary biological aerosol particles in the atmosphere: a review, Tellus Series B-Chemical and Physical Meteorology, 64, 10.3402/tellusb.v64i0.15598, 2012.

Du, C., Liu, S., Yu, X., Li, X., Chen, C., Peng, Y., Dong, Y., Dong, Z., and Wang, F.: Urban Boundary Layer Height Characteristics and Relationship with Particulate Matter Mass Concentrations in Xi'an, Central China, Aerosol and Air Quality Research, 13, 1598-1607, 10.4209/aaqr.2012.10.0274, 2013.

Elbert, W., Taylor, P. E., Andreae, M. O., and Poeschl, U.: Contribution of fungi to primary biogenic aerosols in the atmosphere: wet and dry discharged spores, carbohydrates, and inorganic ions, Atmospheric Chemistry and Physics, 7, 4569-4588, 2007.

Emberlin, J., Newman, T., and Bryant, R.: The incidence of fungal spores in the ambient air and inside homes: Evidence from London, Aerobiologia, 11, 253-258, 10.1007/bf02447205, 1995

Fisher, M. C., Henk, D. A., Briggs, C. J., Brownstein, J. S., Madoff, L. C., McCraw, S. L., and Gurr, S. J.: Emerging fungal threats to animal, plant and ecosystem health, Nature, 484, 186-194, 10.1038/nature10947, 2012.

Fröhlich-Nowoisky, J., Pickersgill, D. A., Desprès, V. R., and Pöschl, U.: High diversity of fungi in air particulate matter, Proceedings of the National Academy of Sciences, 106, 12814-12819, 10.1073/pnas.0811003106, 2009.

Froehlich-Nowoisky, J., Burrows, S. M., Xie, Z., Engling, G., Solomon, P. A., Fraser, M. P., Mayol-Bracero, O. L., Artaxo, P., Begerow, D., Conrad, R., Andreae, M. O., Despres, V. R., and Poeschl, U.: Biogeography in the air: fungal diversity over land and oceans, Biogeosciences, 9, 1125-1136, 10.5194/bg-9-1125-2012, 2012.

Fuzzi, S., Mandrioli, P., and Perfetto, A.: Fog droplets - An atmospheric source of secondary biological aerosol particles, Atmospheric Environment, 31, 287-290, 10.1016/1352-2310(96)00160-4, 1997.

Gabey, A. M., Gallagher, M. W., Whitehead, J., Dorsey, J. R., Kaye, P. H., and Stanley, W. R.: Measurements and comparison of primary biological aerosol above and below a tropical forest canopy using a dual channel fluorescence spectrometer, Atmospheric Chemistry and Physics, 10, 4453-4466, 10.5194/acp-10-4453-2010, 2010.

1011 Gabey, A. M., Stanley, W. R., Gallagher, M. W., and Kaye, P. H.: The fluorescence properties of
1012 aerosol larger than 0.8 mu m in urban and tropical rainforest locations, Atmospheric Chemistry
1013 and Physics, 11, 5491-5504, 10.5194/acp-11-5491-2011, 2011.

1014 Gabey, A. M., Vaitilingom, M., Freney, E., Boulon, J., Sellegri, K., Gallagher, M. W., Crawford,
1015 I. P., Robinson, N. H., Stanley, W. R., and Kaye, P. H.: Observations of fluorescent and
1016 biological aerosol at a high-altitude site in central France, Atmospheric Chemistry and Physics,
1017 13, 7415-7428, 10.5194/acp-13-7415-2013, 2013.

1018 Gangamma, S.: Characteristics of airborne bacteria in Mumbai urban environment, Science of
1019 the Total Environment, 488, 70-74, 10.1016/j.scitotenv2014.04.065, 2014.

1020 Garland, R. M., Schmid, O., Nowak, A., Achtert, P., Wiedensohler, A., Gunthe, S. S., Takegawa,
1021 N., Kita, K., Kondo, Y., Hu, M., Shao, M., Zeng, L. M., Zhu, T., Andreae, M. O., and Poschl, U.:
1022 Aerosol optical properties observed during Campaign of Air Quality Research in Beijing 2006
1023 (CAREBeijing-2006): Characteristic differences between the inflow and outflow of Beijing city
1024 air, Journal of Geophysical Research-Atmospheres, 114, 2009.

1025 Grand, L. F., and Vandyke, C. G.: Scanning electron microscopy of basidiospores of species of
1026 hydnellum, hydnum, phellodon, and bankera (hydnaceae), Journal of the Elisha Mitchell
1027 Scientific Society, 92, 114-123, 1976.

1028 Hairston, P. P., Ho, J., and Quant, F. R.: Design of an instrument for real-time detection of
1029 bioaerosols using simultaneous measurement of particle aerodynamic size and intrinsic
1030 fluorescence, Journal of Aerosol Science, 28, 471-482, 10.1016/s0021-8502(96)00448-x, 1997.

1031 Hallar, A. G., Chirokova, G., McCubbin, I., Painter, T. H., Wiedinmyer, C., and Dodson, C.:
1032 Atmospheric bioaerosols transported via dust storms in the western United States, Geophysical
1033 Research Letters, 38, 10.1029/2011gl048166, 2011.

1034 Hameed, A. A. A., Khoder, M. I., Ibrahim, Y. H., Saeed, Y., Osman, M. E., and Ghanem, S.:
1035 Study on some factors affecting survivability of airborne fungi, Science of the Total
1036 Environment, 414, 696-700, 10.1016/j.scitotenv.2011.10.042, 2012.

1037 Hameed, A. A. A., Khoder, M. I., Yuosra, S., Osman, A. M., and Ghanem, S.: Diurnal
1038 distribution of airborne bacteria and fungi in the atmosphere of Helwan area, Egypt, Science of
1039 the Total Environment, 407, 6217-6222, 10.1016/j.scitotenv.2009.08.028, 2009.

1040 Hara, K., and Zhang, D.: Bacterial abundance and viability in long-range transported dust,
1041 Atmospheric Environment, 47, 20-25, 10.1016/j.atmosenv.2011.11.050, 2012.

1042 Hasnain, S. M.: Influence of meteorological factors on the air spora, Grana, 32, 184-188, 1993.

1043 Healy, D. A., Huffman, J. A., O'Connor, D. J., Poehlker, C., Poeschl, U., and Sodeau, J. R.:
1044 Ambient measurements of biological aerosol particles near Killarney, Ireland: a comparison
1045 between real-time fluorescence and microscopy techniques, Atmospheric Chemistry and Physics,
1046 14, 8055-8069, 10.5194/acp-14-8055-2014, 2014.

1047 Herrero, B., FombellaBlanco, M. A., FernandezGonzalez, D., and ValenciaBarrera, R. M.: The
1048 role of meteorological factors in determining the annual variation of Alternaria and
1049 Cladosporium snores in the atmosphere of Palencia, 1990-1992, International Journal of
1050 Biometeorology, 39, 139-142, 10.1007/bf01211226, 1996.

1051 Hirst, J. M.: Changes in atmospheric spore content: Diurnal periodicity and the effects of
1052 weather, Transactions of the British Mycological Society, 36, 375-IN378,
1053 http://dx.doi.org/10.1016/S0007-1536(53)80034-3, 1953.

1054 Hjelmroos, M.: Relationship between airborne fungal spore presence and weather variables -
1055 cladosporium and alternaria, Grana, 32, 40-47, 1993.

1056 Ho, H. M., Rao, C. Y., Hsu, H. H., Chiu, Y. H., Liu, C. M., and Chao, H. J.: Characteristics and
1057 determinants of ambient fungal spores in Hualien, Taiwan, Atmospheric Environment, 39, 5839-
1058 5850, 10.1016/j.atmonsenv.2005.06.034, 2005.

1059 Hollins, P. D., Kettlewell, P. S., Atkinson, M. D., Stephenson, D. B., Corden, J. M., Millington,
1060 W. M., and Mullins, J.: Relationships between airborne fungal spore concentration of
1061 Cladosporium and the summer climate at two sites in Britain, International Journal of
1062 Biometeorology, 48, 137-141, 10.1007/s00484-003-0188-9, 2004.

1063 Horner, W. E., Oneil, C. E., and Lehrer, S. B.: Basidiospore aeroallergens, Clinical Reviews in
1064 Allergy, 10, 191-211, 1992.

1065 Huffman, J. A., Treutlein, B., and Pöschl, U.: Fluorescent biological aerosol particle
1066 concentrations and size distributions measured with an Ultraviolet Aerodynamic Particle Sizer
1067 (UV-APS) in Central Europe, Atmos. Chem. Phys., 10, 3215-3233, 2010.

1068 Huffman, J. A., Sinha, B., Garland, R. M., Snee-Pollmann, A., Gunthe, S. S., Artaxo, P., Martin,
1069 S. T., Andreae, M. O., and Poschl, U.: Size distributions and temporal variations of biological
1070 aerosol particles in the Amazon rainforest characterized by microscopy and real-time UV-APS
1071 fluorescence techniques during AMAZE-08, Atmospheric Chemistry and Physics, 12, 11997-
1072 12019, 10.5194/acp-12-11997-2012, 2012.

1073 Huffman, J. A., Prenni, A. J., DeMott, P. J., Poehlker, C., Mason, R. H., Robinson, N. H.,
1074 Froehlich-Nowoisky, J., Tobo, Y., Despres, V. R., Garcia, E., Gochis, D. J., Harris, E., Mueller-
1075 Germann, I., Ruzene, C., Schmer, B., Sinha, B., Day, D. A., Andreae, M. O., Jimenez, J. L.,
1076 Gallagher, M., Kreidenweis, S. M., Bertram, A. K., and Poeschl, U.: High concentrations of
1077 biological aerosol particles and ice nuclei during and after rain, Atmospheric Chemistry and
1078 Physics, 13, 6151-6164, 10.5194/acp-13-6151-2013, 2013.

1079 Jones, A. M., and Harrison, R. M.: The effects of meteorological factors on atmospheric
1080 bioaerosol concentrations - a review, Science of the Total Environment, 326, 151-180,
1081 10.1016/j.scitotenv.2003.11.021, 2004.

1082 Kanaani, H., Hargreaves, M., Ristovski, Z., and Morawska, L.: Performance assessment of
1083 UVAPS: Influence of fungal spore age and air exposure, Journal of Aerosol Science, 38, 83-96,
1084 10.1016/j.jaerosci.2006.10.003, 2007.

Kanaani, H., Hargreaves, M., Smith, J., Ristovski, Z., Agranovski, V., and Morawska, L.: Performance of UVAPS with respect to detection of airborne fungi, Journal of Aerosol Science, 39, 175-189, 10.1016/j.jaerosci.2007.10.007, 2008.

Kanawade, V. P., Shika, S., Poehlker, C., Rose, D., Suman, M. N. S., Gadhavi, H., Kumar, A., Nagendra, S. M. S., Ravikrishna, R., Yu, H., Sahu, L. K., Jayaraman, A., Andreae, M. O., Poeschl, U., and Gunthe, S. S.: Infrequent occurrence of new particle formation at a semi-rural location, Gadanki, in tropical Southern India, Atmospheric Environment, 94, 264-273, 10.1016/j.atmosenv.2014.05.046, 2014.

Kurkela, T.: The number of Cladosporium conidia in the air in different weather conditions, Grana, 36, 54-61, 1997.

Lee, S.-H., Lee, H.-J., Kim, S.-J., Lee, H. M., Kang, H., and Kim, Y. P.: Identification of airborne bacterial and fungal community structures in an urban area by T-RFLP analysis and quantitative real-time PCR, Science of the Total Environment, 408, 1349-1357, 10.1016/j.scitotenv.2009.10.061, 2010.

Levetin, E., and Horner, W. E.: Fungal aerobiology: Exposure and measurement, Fungal Allergy and Pathogenicity, 81, 10-27, 2002.

Li, D. W., and Kendrick, B.: Functional-relationships between airborne fungal spores and environmental-factors in Kitchener-Waterloo, Ontario, as detected by canonical correspondence-analysis, Grana, 33, 166-176, 1994.

Li, F., and Ramanathan, V.: Winter to summer monsoon variation of aerosol optical depth over the tropical Indian Ocean, Journal of Geophysical Research-Atmospheres, 107, 10.1029/2001jd000949, 2002.

Li, M., Qi, J., Zhang, H., Huang, S., Li, L., and Gao, D.: Concentration and size distribution of bioaerosols in an outdoor environment in the Qingdao coastal region, Science of the Total Environment, 409, 3812-3819, 10.1016/j.scitotenv.2011.06.001, 2011.

Lyon, F. L., Kramer, C. L., and Eversmeyer, M. G.: Variation of airspora in the atmosphere due to weather conditions, Grana, 23, 177-181, 1984.

Madden, L. V.: Effects of rain on splash dispersal of fungal pathogens, Canadian Journal of Plant Pathology, 19, 225-230, 1997.

Maki, T., Kakikawa, M., Kobayashi, F., Yamada, M., Matsuki, A., Hasegawa, H., and Iwasaka, Y.: Assessment of composition and origin of airborne bacteria in the free troposphere over Japan, Atmospheric Environment, 74, 73-82, 10.1016/j.atmosenv.2013.03.029, 2013.

Matthias-Maser, S., Obolkin, V., Khodzer, T., and Jaenicke, R.: Seasonal variation of primary biological aerosol particles in the remote continental region of Lake Baikal/Siberia, Atmospheric Environment, 34, 3805-3811, 10.1016/s1352-2310(00)00139-4, 2000.

Matthiasmaser, S., and Jaenicke, R.: A method to identify biological aerosol-particles with radius greater-than 0.3 μm for the determination of their size distribution, Journal of Aerosol Science, 22, S849-S852, 10.1016/s0021-8502(05)80232-0, 1991.

Matthiasmaser, S., and Jaenicke, R.: Examination of atmospheric bioaerosol particles with radii greater-than-0.2 μm, Journal of Aerosol Science, 25, 1605-1613, 10.1016/0021-8502(94)90228-3, 1994.

MatthiasMaser, S., and Jaenicke, R.: The size distribution of primary biological aerosol particles with radii >0.2 μm in an urban rural influenced region, Atmospheric Research, 39, 279-286, 10.1016/0169-8095(95)00017-8, 1995.

Moehler, O., DeMott, P. J., Vali, G., and Levin, Z.: Microbiology and atmospheric processes: the role of biological particles in cloud physics, Biogeosciences, 4, 1059-1071, 2007.

Moorthy, K. K., Nair, P. R., and Murthy, B. V. K.: Size distribution of coastal aerosols - effects of local-sources and sinks, Journal of Applied Meteorology, 30, 844-852, 10.1175/1520-0450(1991)030<0844:sdocae>2.0.co;2, 1991.

Morris, C. E., Georgakopoulos, D. G., and Sands, D. C.: Ice nucleation active bacteria and their potential role in precipitation, Journal De Physique Iv, 121, 87-103, 10.1051/jp4:2004121004, 2004.

Morris, C. E., Conen, F., Huffman, J. A., Phillips, V., Poeschl, U., and Sands, D. C.: Bioprecipitation: a feedback cycle linking Earth history, ecosystem dynamics and land use through biological ice nucleators in the atmosphere, Global Change Biology, 20, 341-351, 10.1111/gcb.12447, 2014.

Myers, N., Mittermeier, R. A., Mittermeier, C. G., da Fonseca, G. A. B., and Kent, J.: Biodiversity hotspots for conservation priorities, Nature, 403, 853-858, 10.1038/35002501, 2000.

Naja, M., and Lal, S.: Surface ozone and precursor gases at Gadanki (13.5 degrees N, 79.2 degrees E), a tropical rural site in India, Journal of Geophysical Research-Atmospheres, 107, 10.1029/2001jd000357, 2002.

Oh, J.-W., Lee, H.-B., Lee, H.-R., Pyun, B.-Y., Ahn, Y.-M., Kim, K.-E., Lee, S.-Y., and Lee, S.-I.: Aerobiological study of pollen and mold in Seoul, Korea, Allergology International, 47, 263-270, http://dx.doi.org/10.2332/allergolint.47.263, 1998.

Oliveira, M., Amorim, M. I., Ferreira, E., Delgado, L., and Abreu, I.: Main airborne Ascomycota spores: characterization by culture, spore morphology, ribosomal DNA sequences and enzymatic analysis, Applied Microbiology and Biotechnology, 86, 1171-1181, 10.1007/s00253-010-2448-z, 2010.

Pachauri, T., Singla, V., Satsangi, A., Lakhani, A., and Kumari, K. M.: Characterization of major pollution events (dust, haze, and two festival events) at Agra, India, Environmental Science and Pollution Research, 20, 5737-5752, 10.1007/s11356-013-1584-2, 2013.

Pan, Y. L., Holler, S., Chang, R. K., Hill, S. C., Pinnick, R. G., Niles, S., and Bottiger, J. R.: Single-shot fluorescence spectra of individual micrometer-sized bioaerosols illuminated by a 351- or a 266-nm ultraviolet laser, Optics Letters, 24, 116-118, 10.1364/ol.24.000116, 1999a.

Pan, Y. L., Holler, S., Chang, R. K., Hill, S. C., Pinnick, R. G., Niles, S., Bottiger, J. R., and Bronk, B. V.: Real-time detection and characterization of individual flowing airborne biological particles: fluorescence spectra and elastic scattering measurements, in: Air Monitoring and Detection of Chemical and Biological Agents Ii, edited by: Leonelli, J., and Althouse, M. L., Proceedings of the Society of Photo-Optical Instrumentation Engineers (Spie), 117-125, 1999b.

Poehlker, C., Huffman, J. A., and Poeschl, U.: Auto fluorescence of atmospheric bioaerosols - fluorescent biomolecules and potential interferences, Atmospheric Measurement Techniques, 5, 37-71, 10.5194/amt-5-37-2012, 2012.

Poehlker, C., Huffman, J. A., Foerster, J. D., and Poeschl, U.: Auto fluorescence of atmospheric bioaerosols: spectral fingerprints and taxonomic trends of pollen, Atmospheric Measurement Techniques, 6, 3369-3392, 10.5194/amt-6-3369-2013, 2013.

Poschl, U.: Atmospheric aerosols: Composition, transformation, climate and health effects, Angewandte Chemie-International Edition, 44, 7520-7540, 10.1002/anie.200501122, 2005.

Pöschl, U., Martin, S. T., Sinha, B., Chen, Q., Gunthe, S. S., Huffman, J. A., Borrmann, S., Farmer, D. K., Garland, R. M., Helas, G., Jimenez, J. L., King, S. M., Manzi, A., Mikhailov, E., Pauliquevis, T., Petters, M. D., Prenni, A. J., Roldin, P., Rose, D., Schneider, J., Su, H., Zorn, S. R., Artaxo, P., and Andreae, M. O.: Rainforest Aerosols as Biogenic Nuclei of Clouds and Precipitation in the Amazon, Science, 329, 1513-1516, 10.1126/science.1191056, 2010.

Pranesha, T. S., and Kamra, A. K.: Scavenging of aerosol particles by large water drops .2. The effect of electrical forces, Journal of Geophysical Research-Atmospheres, 102, 23937-23946, 10.1029/97jd01834, 1997a.

Pranesha, T. S., and Kamra, A. K.: Scavenging of aerosol particles by large water drops .3. Washout coefficients, half-lives, and rainfall depths, Journal of Geophysical Research-Atmospheres, 102, 23947-23953, 10.1029/97jd01835, 1997b.

Prenni, A. J., Petters, M. D., Kreidenweis, S. M., Heald, C. L., Martin, S. T., Artaxo, P., Garland, R. M., Wollny, A. G., and Poschl, U.: Relative roles of biogenic emissions and Saharan dust as ice nuclei in the Amazon basin, Nature Geoscience, 2, 401-404, 2009.

Prenni, A. J., Tobo, Y., Garcia, E., DeMott, P. J., Huffman, J. A., McCluskey, C. S., Kreidenweis, S. M., Prenni, J. E., Poehlker, C., and Poeschl, U.: The impact of rain on ice nuclei populations at a forested site in Colorado, Geophysical Research Letters, 40, 227-231, 10.1029/2012gl053953, 2013.

Prospero, J. M.: Mineral and sea salt aerosol concentrations in various ocean regions, Journal of Geophysical Research-Oceans and Atmospheres, 84, 725-731, 10.1029/JC084iC02p00725, 1979.

Prospero, J. M., Blades, E., Mathison, G., and Naidu, R.: Inter-hemispheric transport of viable fungi and bacteria from Africa to the Caribbean with soil dust, Aerobiologia, 21, 1-19, 10.1007/s10453-004-5872-7, 2005.

Quintero, E., Rivera-Mariani, F., and Bolanos-Rosero, B.: Analysis of environmental factors and their effects on fungal spores in the atmosphere of a tropical urban area (San Juan, Puerto Rico), Aerobiologia, 26, 113-124, 10.1007/s10453-009-9148-0, 2010.

Raatikainen, T., Hyvarinen, A. P., Hatakka, J., Panwar, T. S., Hooda, R. K., Sharma, V. P., and Lihavainen, H.: The effect of boundary layer dynamics on aerosol properties at the Indo-Gangetic plains and at the foothills of the Himalayas, Atmospheric Environment, 89, 548-555, 10.1016/j.atmosenv.2014.02.058, 2014.

Radke, L. F., Hobbs, P. V., and Eltgroth, M. W.: Scavenging of aerosol-particles by precipitation, Journal of Applied Meteorology, 19, 715-722, 10.1175/1520-0450(1980)019<0715:soapbp>2.0.co;2, 1980.

Saari, S., Niemi, J. V., Ronkko, T., Kuuluvainen, H., Jarvinen, A., Pirjola, L., Aurela, M., Hillamo, R., and Keskinen, J.: Seasonal and Diurnal Variations of Fluorescent Bioaerosol Concentration and Size Distribution in the Urban Environment, Aerosol and Air Quality Research, 15, 572-581, 10.4209/aaqr.2014.10.0258, 2015.

Saari, S., Reponen, T., and Keskinen, J.: Performance of Two Fluorescence - Based Real-Time Bioaerosol Detectors: Bioscout vs. UVAPS, Aerosol Sci. Technol, 48, 371-378, 10.1080/02786826.2013.877579, 2014.

Sabariego, S., de la Guardia, C. D., and Alba, F.: The effect of meteorological factors on the daily variation of airborne fungal spores in Granada (southern Spain), International Journal of Biometeorology, 44, 1-5, 10.1007/s004840050131, 2000.

Sadys, M., Skjoth, C. A., and Kennedy, R.: Back-trajectories show export of airborne fungal spores (Ganoderma sp.) from forests to agricultural and urban areas in England, Atmospheric Environment, 84, 88-99, 10.1016/j.atmosenv.2013.11.015, 2014.

Santarpia, J. L., Ratnesar-Shumate, S., Gilberry, J. U., and Quizon, J. J.: Relationship Between Biologically Fluorescent Aerosol and Local Meteorological Conditions, Aerosol Sci. Technol., 47, 655-661, 10.1080/02786826.2013.781263, 2013.

Satheesh, S. K., and Srinivasan, J.: Enhanced aerosol loading over Arabian Sea during the pre-monsoon season: Natural or anthropogenic?, Geophysical Research Letters, 29, 10.1029/2002gl015687, 2002.

Schumacher, C. J., Poehlker, C., Aalto, P., Hiltunen, V., Petaja, T., Kulmala, M., Poeschl, U., and Huffman, J. A.: Seasonal cycles of fluorescent biological aerosol particles in boreal and semi-arid forests of Finland and Colorado, Atmospheric Chemistry and Physics, 13, 11987-12001, 10.5194/acp-13-11987-2013, 2013.

1229 Sesartic, A., and Dallafior, T. N.: Global fungal spore emissions, review and synthesis of
1230 literature data, Biogeosciences, 8, 1181-1192, 10.5194/bg-8-1181-2011, 2011.

1231 Shaffer, B. T., and Lighthart, B.: Survey of culturable airborne bacteria at four diverse locations
1232 in Oregon: Urban, rural, forest, and coastal, Microbial Ecology, 34, 167-177,
1233 10.1007/s002489900046, 1997.

1234 Sharma, N. K., and Rai, A. K.: Allergenicity of airborne cyanobacteria Phormidium fragile and
1235 Nostoc muscorum, Ecotoxicology and Environmental Safety, 69, 158-162,
1236 10.1016/j.ecoenv.2006.08.006, 2008.

1237 Sherman, J. P., Sheridan, P. J., Ogren, J. A., Andrews, E., Hageman, D., Schmeisser, L.,
1238 Jefferson, A., and Sharma, S.: A multi-year study of lower tropospheric aerosol variability and
1239 systematic relationships from four North American regions, Atmospheric Chemistry and Physics,
1240 15, 12487-12517, 10.5194/acp-15-12487-2015, 2015.

1241 Shika, S., et al.: Atmospheric aerosol properties at a semi-rural location in South India: particle
1242 size distributions and implications for cloud formation, to be submitted.

1243 Sivaprakasam, V., Huston, A. L., Scotto, C., and Eversole, J. D.: Multiple UV wavelength
1244 excitation and fluorescence of bioaerosols, Optics Express, 12, 4457-4466,
1245 10.1364/opex.12.004457, 2004.

1246 Spracklen, D. V., and Heald, C. L.: The contribution of fungal spores and bacteria to regional
1247 and global aerosol number and ice nucleation immersion freezing rates, Atmospheric Chemistry
1248 and Physics, 14, 9051-9059, 10.5194/acp-14-9051-2014, 2014.

1249 Srivastava, A., Singh, M., and Jain, V. K.: Identification and characterization of size-segregated
1250 bioaerosols at Jawaharlal Nehru University, New Delhi, Natural Hazards, 60, 485-499,
1251 10.1007/s11069-011-0022-3, 2012.

1252 Tarlo, S. M., Bell, B., Srinivasan, J., Dolovich, J., and Hargreave, F. E.: Human sensitization to
1253 ganoderma antigen, Journal of Allergy and Clinical Immunology, 64, 43-49, 10.1016/0091-
1254 6749(79)90082-4, 1979.

1255 Tong, Y and Lighthart, B.: Diurnal Distribution of Total and Culturable Atmospheric Bacteria at
1256 a Rural Site, Aerosol Sci. Technol., 30, 246-254, 10.1080/027868299304822, 1999.

1257 Toprak, E., and Schnaiter, M.: Fluorescent biological aerosol particles measured with the
1258 Waveband Integrated Bioaerosol Sensor WIBS-4: laboratory tests combined with a one year
1259 field study, Atmospheric Chemistry and Physics, 13, 225-243, 10.5194/acp-13-225-2013, 2013.

1260 Trejo, M., Douarche, C., Bailleux, V., Poulard, C., Mariot, S., Regeard, C., and Raspaud, E.:
1261 Elasticity and wrinkled morphology of Bacillus subtilis pellicles, Proceedings of the National
1262 Academy of Sciences of the United States of America, 110, 2011-2016,
1263 10.1073/pnas.1217178110, 2013.

Troutt, C., and Levetin, E.: Correlation of spring spore concentrations and meteorological conditions in Tulsa, Oklahoma, International Journal of Biometeorology, 45, 64-74, 10.1007/s004840100087, 2001.

Valsan, A. E., Priyamvada, H., Ravikrishna, R., Després, V. R., Biju, C. V., Sahu, L. K., Kumar, A., Verma, R. S., Philip, L., and Gunthe, S. S.: Morphological characteristics of bioaerosols from contrasting locations in southern tropical India – A case study, Atmospheric Environment, 122, 321-331, http://dx.doi.org/10.1016/j.atmosenv.2015.09.071, 2015.

Vinoj, V., and Satheesh, S. K.: Measurements of aerosol optical depth over Arabian Sea during summer monsoon season, Geophysical Research Letters, 30, 10.1029/2002gl016664, 2003.

Vinoj, V., Satheesh, S. K., and Moorthy, K. K.: Optical, radiative, and source characteristics of aerosols at Minicoy, a remote island in the southern Arabian Sea, Journal of Geophysical Research-Atmospheres, 115, 10.1029/2009jd011810, 2010.

Vinoj, V., Rasch, P. J., Wang, H., Yoon, J.-H., Ma, P.-L., Landu, K., and Singh, B.: Short-term modulation of Indian summer monsoon rainfall by West Asian dust, Nature Geoscience, 7, 308-313, 10.1038/ngeo2107, 2014.

Wang, C.-C., Fang, G.-C., and Lee, L.: Bioaerosols study in central Taiwan during summer season, Toxicology and Industrial Health, 23, 133-139, 10.1177/0748233707078741, 2007.

Yu, X., Wang, Z., Zhang, M., Kuhn, U., Xie, Z., Cheng, Y., Pöschl, U., and Su, H.: Ambient measurement of fluorescent aerosol particles with a WIBS in the Yangtze River Delta of China: potential impacts of combustion-generated aerosol particles, Atmos. Chem. Phys. Discuss., doi:10.5194/acp-2016-228, in review, 2016.

Zhang, T., Engling, G., Chan, C.-Y., Zhang, Y.-N., Zhang, Z.-S., Lin, M., Sang, X.-F., Li, Y. D., and Li, Y.-S.: Contribution of fungal spores to particulate matter in a tropical rainforest, Environmental Research Letters, 5, 10.1088/1748-9326/5/2/024010, 2010.

Table 1: List of frequently used acronyms and symbols with units.

Symbol	Quantity, Unit
D_a	Aerodynamic diameter, μm
D_g	Geometric midpoint diameter of fluorescent particles
$D_{g,T}$	Geometric midpoint diameter of total particles
DNA	Deoxyribonucleic acid
FBAP	Fluorescent biological aerosol particle
He-Ne	Helium-Neon
ITCZ	Inter Tropical Convergence Zone
Lpm	Liters per minute
M_F	Integrated mass concentration of fluorescent particles, μg m^{-3}
M_T	Integrated mass concentration of total particles, μg m^{-3}
Nd:YAG	Neodymium-doped yttrium Aluminum garnet
NE	Northeast
N_F	Integrated number concentration of fluorescent particles, cm^{-3}
N_T	Integrated number concentration of total particles, cm^{-3}
PAH	Polycyclic aromatic hydrocarbon
PBAPs	Primary Biological Aerosol Particles
RH	Relative Humidity
SEM	Scanning Electron Microscopy
SW	Southwest
TAP	Total Aerosol Particle
TSP	Total Suspended Particle
UV-APS	Ultraviolet Aerodynamic Particle Sizer
λ	Wavelength, nm

Number		June	July	August	Campaign
N_T (cm^{-3})	Mean	2.66	1.54	0.96	1.77
	Median	2.45	1.48	0.73	1.44
N_F (cm^{-3})	Mean	0.03	0.007	0.015	0.017
	Median	0.02	0.006	0.007	0.01
N_F/N_T (%)	Mean	0.03	0.01	0.03	0.02
	Median	0.01		0.01	0.01
Mass		June	July	August	Campaign
M_T (µg m^{-3})	Mean	10.61	6.15	4.15	7.17
	Median	9.58	5.55	2.8	5.57
M_F (µg m^{-3})	Mean	0.42	0.11	0.18	0.24
	Median	0.33	0.09	0.1	0.15
M_F/M_T (%)	Mean	0.09	0.03	0.08	0.06
	Median	0.04	0.02	0.03	0.03

Table 2: Integrated number concentrations and mass concentrations of coarse TAP and FBAP (~1–20 µm): arithmetic mean and median for each month and for the entire measurement campaign

Sl No:	Location	Land Use	Measurement Period	Season	Instrument	FBAP Number Concentration	Total Number Concentration	Number Ratio (%)	Reference
1	Mainz, Central Europe	Semi-urban	Aug-Dec, 2006		UVAPS	3×10^{-2} cm^{-3}	1.05 cm^{-3}	4	Huffman et al., 2010
2	Central Amazonia rainforest	Tropical rainforest	Feb-Mar, 2008		UVAPS	7.3×10^{-2} cm^{-3}	0.33 cm^{-3}	24	Huffman et al., 2012
3	Manchester, UK	Urban	December, 2009		WIBS-3	2.9×10^{-4} cm^{-3} (FL1)	1.38×10^{-2} cm^{-3}	2.1	Gabey et al., 2011
						5.2×10^{-4} cm^{-3} (FL2)		3.7	
						1.1×10^{-5} cm^{-3} (FL3)		7.8	
4	Central France	Rural	22 Jun-3 July, 2010		WIBS-3	1.2×10^{-2} cm^{-3} (280 nm)			Gabey et al., 2013
						9.5×10^{-2} cm^{-3} (370 nm)			
5	Helinski, Finland	Urban	Feb, 2012 (Winter)	Winter	BioScout	1×10^{-2} cm^{-3}		23	Saari et al., 2015
			June-Aug, 2012 (Summer)	Summer		2.8×10^{-2} cm^{-3}		6	
				Summer	UVAPS	1.3×10^{-2} cm^{-3}		8	
6	Colorado, USA	Pine forest	June-July,2011	Dry period	WIBS-3			5.8	Crawford et al., 2014
				Wet Period	WIBS-4			15.2	
7	Finland	Rural forest	August,2009 - April,2011	Spring	UVAPS	1.5×10^{-2} cm^{-3}	0.43 cm^{-3}	4.4	Schumacher et al., 2013
				Summer		4.6×10^{-2} cm^{-3}	0.45 cm^{-3}	13	
				Fall		2.7×10^{-2} cm^{-3}	0.41 cm^{-3}	9.8	
				Winter		0.4×10^{-2} cm^{-3}	0.47 cm^{-3}	1.1	

	Colorado , USA	Rural, semi-arid	2011-2012	Spring	UVAPS	1.5 x 10^{-2} cm^{-3}	0.73 cm^{-3}	2.5	
				Summer		3 x 10^{-2} cm^{-3}	0.44 cm^{-3}	8.8	
				Fall		1.7 x 10^{-2} cm^{-3}	0.28 cm^{-3}	5.7	
				Winter		0.53 x 10^{-2} cm^{-3}	0.2 cm^{-3}	3	
8	Karlsruhe, Germany	Semi-rural	April 2010 - April 2011		WIBS - 4	3.1 x 10^{-2} cm^{-3}	0.583 cm^{-3}	7.34	Toprak and Schnaiter., 2013
9	Nanjing, China	Sub-urban	Oct-Nov, 2013	Autumn	WIBS-4	0.6 cm^{-3} (FL1)	13.1 cm^{-3}	4.6	Yu et al., 2016
						3.4 cm^{-3} (FL2)		25.3	
						2.1 cm^{-3} (FL3)		15.6	

Table 3: Comparison with other online measurements carried out under various environmental conditions across the globe.

Number		Dusty	Clean	High Bio
N_T (cm^{-3})	Mean	4.2	1.27	1.78
	Median	4.36	1.15	1.4
N_F(cm^{-3})	Mean	0.02	0.005	0.05
	Median	0.019	0.004	0.038
N_F/N_T	Mean	0.01	0.01	0.05
	Median			0.03
Mass		Dusty	Clean	High Bio
M_T (μg m^{-3})	Mean	16.34	5.12	7.7
	Median	16.84	4.28	5.85
M_F (μg m^{-3})	Mean	0.36	0.08	0.58
	Median	0.33	0.05	0.47
M_F/M_T	Mean	0.02	0.03	0.12
	Median	0.02	0.01	0.08

Table 4: Integrated number concentrations and mass concentrations of coarse TAP and FBAP (~1–20 μm): arithmetic mean and median for each focus period (Dusty, Clean and High Bio).

	Campaign			Dusty			Clean			High Bio		
	N_T	N_F	N_F/N_T	N_T	N_F	N_F/N_T	N_T	N_F	N_F/N_T	N_T	N_F	N_F/N_T
RH	-0.64	0.58	0.85	-0.25		0.18	-0.66	-0.01	0.13	-0.64	0.5	0.68
Temperature	0.45	-0.65	-0.82	0.34	-0.04	-0.25	0.78	0.02	-0.2	0.43	-0.68	-0.83
Wind Speed	0.4	-0.6	-0.78	0.09	-0.18	-0.31	-0.18	-0.27	0	0.3	-0.61	-0.74

Table 5: R^2 values for correlation between meteorological parameters (RH, Temperature and Wind Speed) and N_T, N_F and N_F/N_T during the entire campaign and each focus periods.

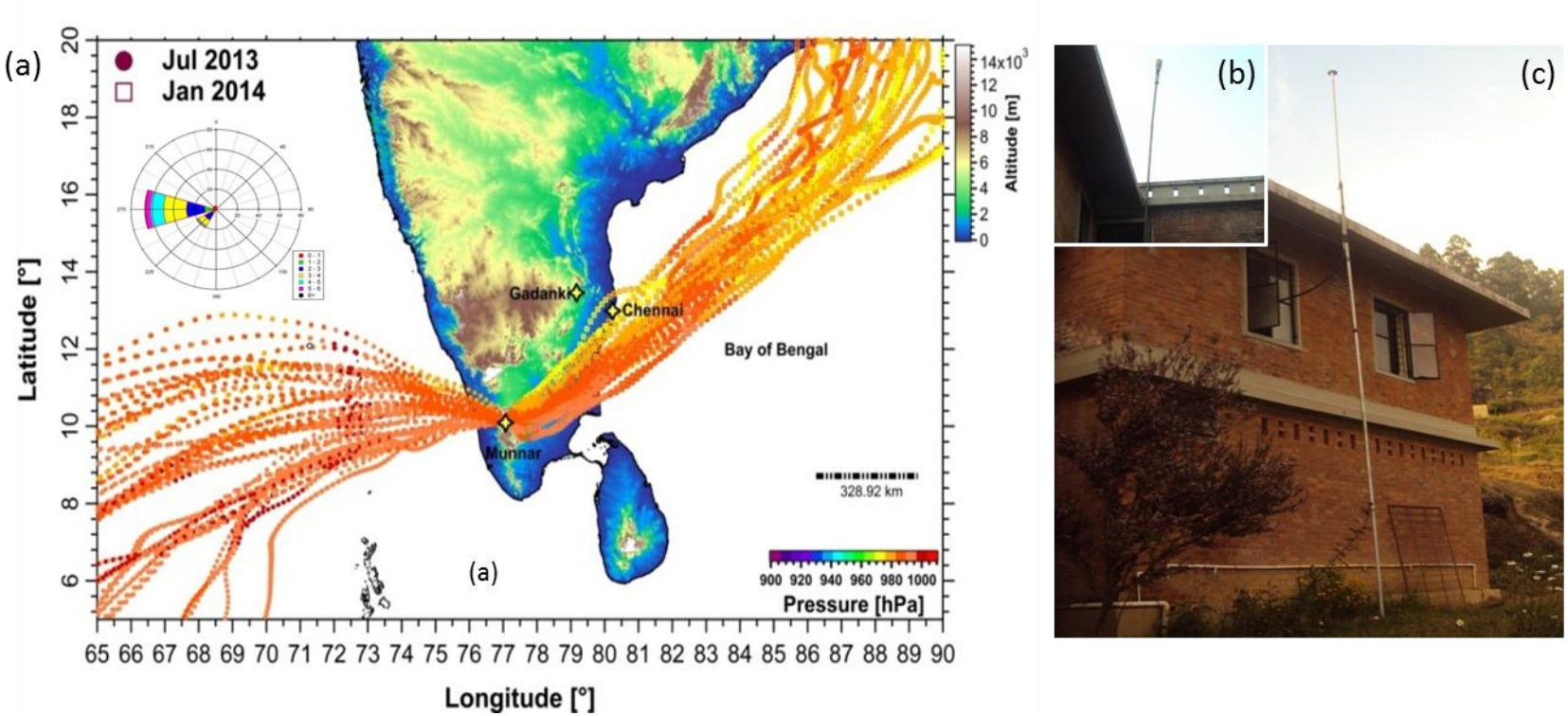

Figure 1: Location of measurement site Munnar (10.09°N, 77.06°E; 1605 m amsl – above mean sea level) located in the Western Ghats mountain range in Southern tropical India with 10 days back trajectories (HYSPLIT, NOAA-ARL GDAS1 model; start height 50 m above ground level; starting time 23:30 local time) illustrating the distinct and contrasting wind patterns during two contrasting seasons; Southwest monsoon season (representative month Jul) and Winter season (representative month Jan) when field measurement campaigns were carried out. It is evident that predominant wind pattern during Southwest monsoon season was Westerly/Southwesterly bringing the clean marine influx as also evident from the wind rose diagram shown in inset(a). The meteorological parameters were recorded using the weather station installed close to the inlet system (b). The inlet system prepared for sampling the air using Ultraviolet Aerodynamic Particle Sizer (UV-APS) for bioaerosol number size distribution measurement (c). The map shown is color-coded by topography (meters) and trajectories are color-coded by atmospheric pressure level (hPa)

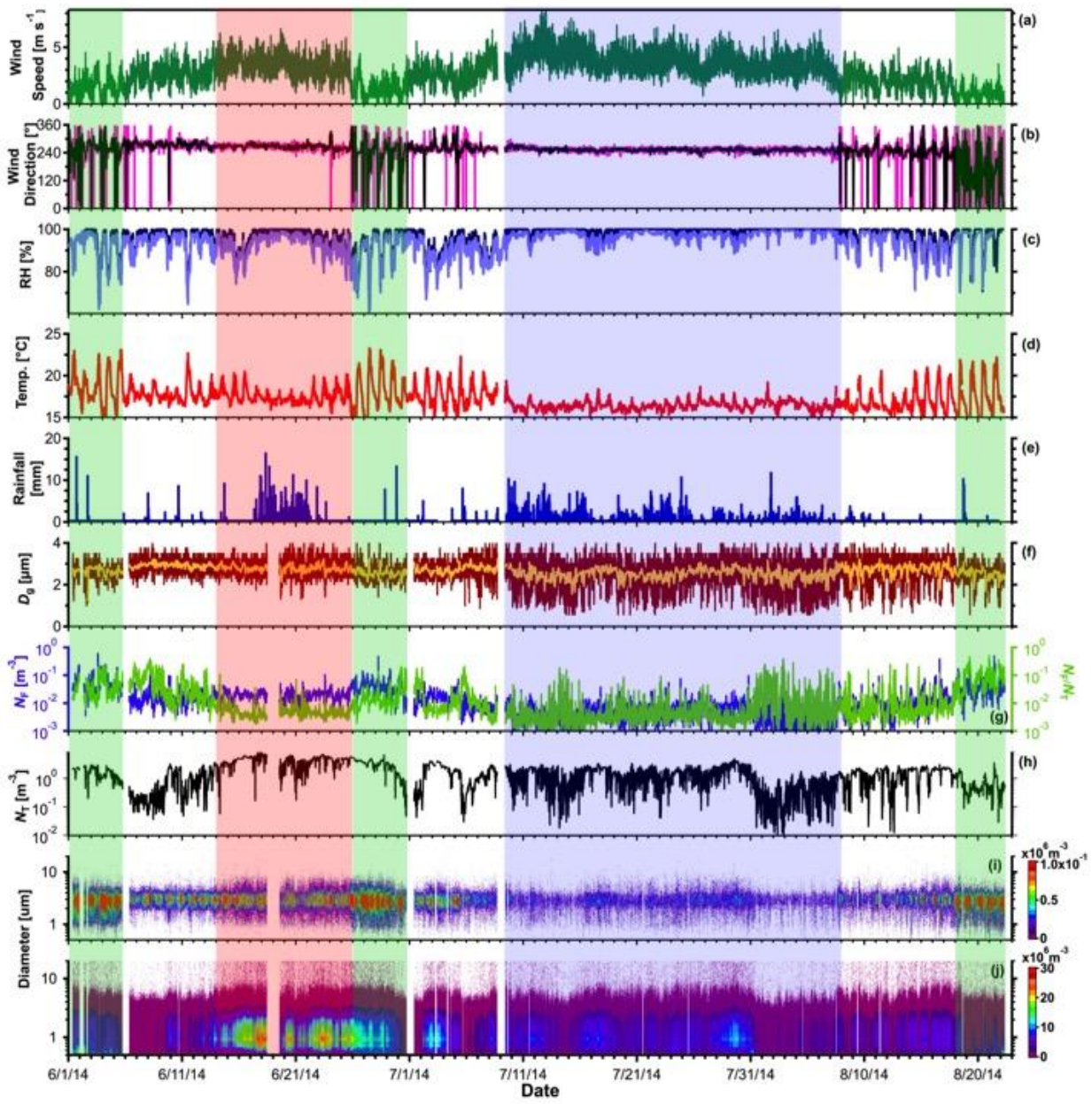

Figure 2: Time series of measured meteorological parameters, parameters derived from FBAP and total particle number size distribution measurements using UV-APS: (a) wind speed, (b) wind direction: five minutes average (magenta) and one hour average (black), (c) relative humidity, (d) temperature, (e) rainfall, (f) geometric mean diameter (D_g) five minutes average (dark red) and one hour average (yellow), (g) FBAP number concentration (N_F; blue) and relative contribution of FBAP to TAP (N_F/N_T; green), (h) TAP number concentration (N_T), (i) a contour plot of FBAP number size distribution (dN/dlog D_F), and (j) a contour plot of TAP number size distribution (dN/dlog D_T). The shadowed block represents the different focus periods (red for dusty; green for high bio; blue for clean: please refer to text for more details).

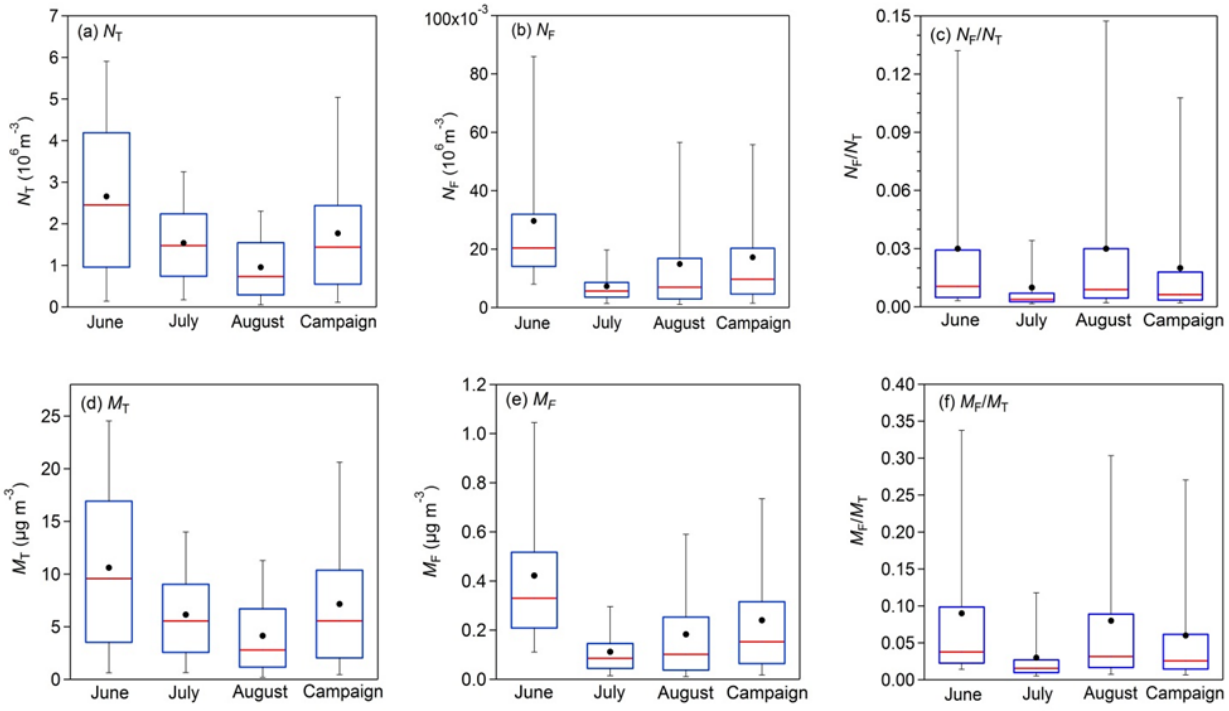

Figure 3: Statistical distribution of integrated (~1 – 20 μm) FBAP and TAP number and mass and their ratios measured during each month (Jun – Aug) of SW monsoon season and averaged over the entire measurement campaign carried out at Munnar as box whisker plots: (a) TAP number concentration (N_T), (b) FBAP number concentration (N_F), (c) contribution of FBAP number concentration to TAP number concentration (N_F/N_T), (d) TAP mass concentration (M_T), (e) FBAP mass concentration (M_F) and (f) contribution of FBAP to TAP mass concentration (M_F/M_T).

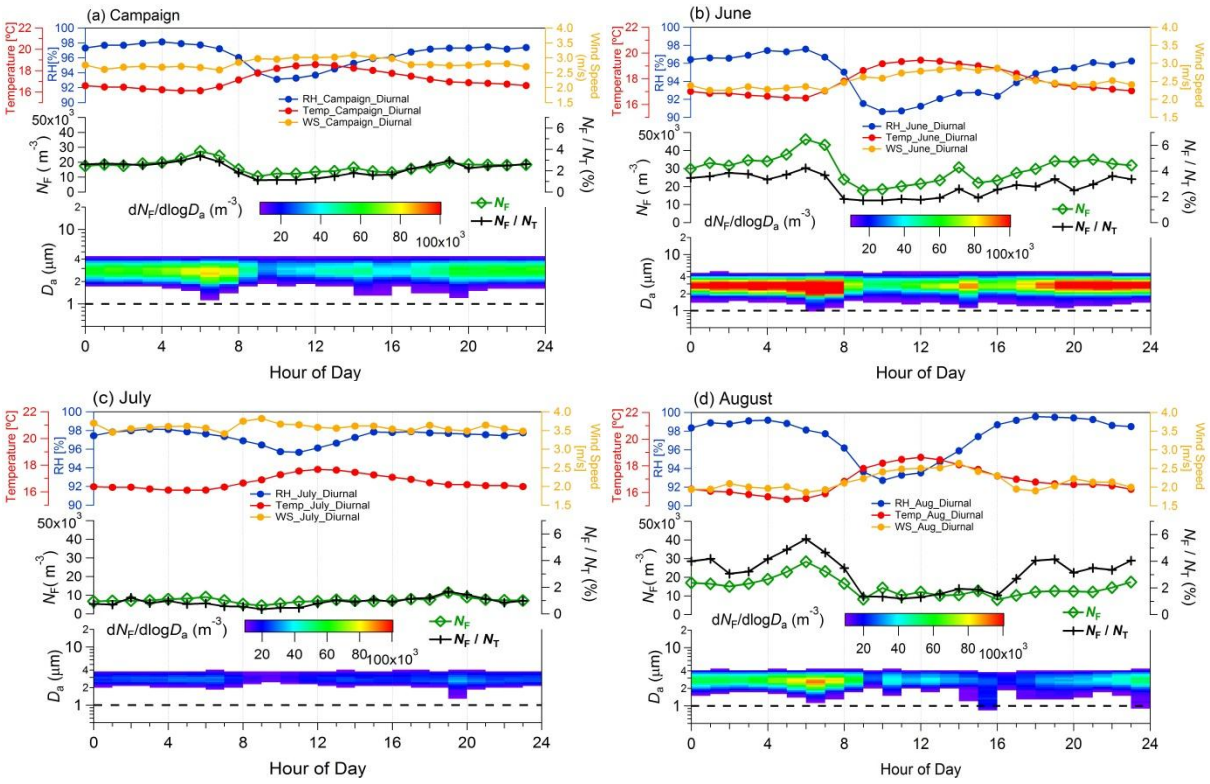

Figure 4: Diurnal cycles of observed meteorological parameters, FBAP number concentrations (N_F) and size distributions averaged over individual month of measurement and entire campaign (hourly mean values plotted against the local time of the day). Upper portion of each panel shows the observed meteorological parameters: relative humidity (%; blue), temperature (°C; red), and wind speed (m s^{-1}; orange on right axis). Middle panel shows integrated FBAP number concentration (~1 – 20 µm; N_F) on the left axis (green color) and FBAP fraction of TAP number (N_F/N_T) on the right axis (black color). Lower portion of each panel FBAP number size distribution (3-D plot) plotted against hour of the day on x-axis, aerodynamic diameter on y-axis and color is scaled for dN_F/dlog D_a indicates the concentration. Dashed black lines in lower portion of the each panel at 1.0 µm shows the particle size cut-off diameter below which fluorescent particles were not considered as FBAP due to potential interference with non-biological aerosol particles. (a) averaged over entire campaign,(b) Jun, (c) Jul, and (d) Aug. Please refer to supplementary Figs. for corresponding TAP plots.

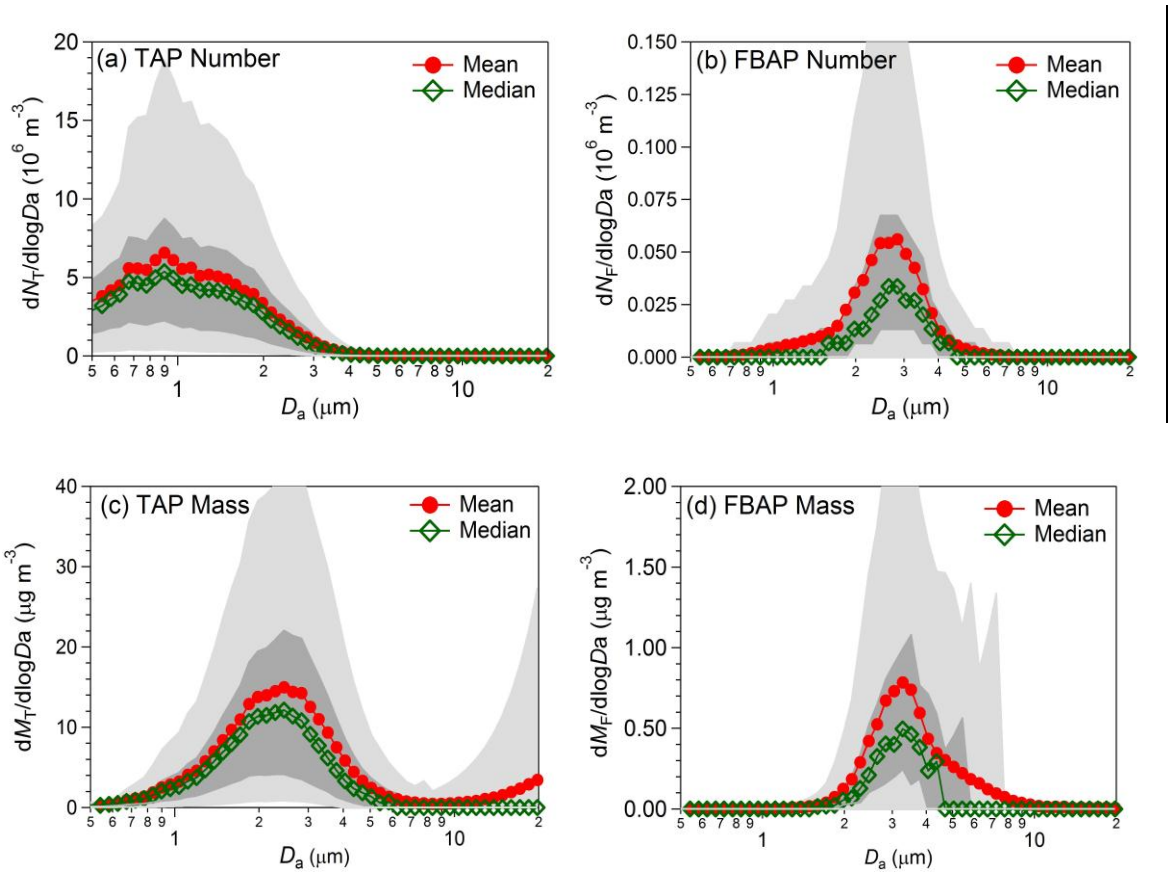

Figure 5: Particle number size and unit-normalized number size and mass size distributions averaged over the entire measurement campaign carried out at Munnar. Lower and upper parts of dark and light shaded area represents the 5^{th}, 25^{th}, 75^{th}, and 95^{th} percentile respectively. (a) TAP number ($dN_T/d\log D_a$), (b) FBAP number ($dN_F/d\log D_a$), (c) total mass ($dM_T/d\log D_a$), and (d) FBAP mass ($dM_F/d\log D_a$).

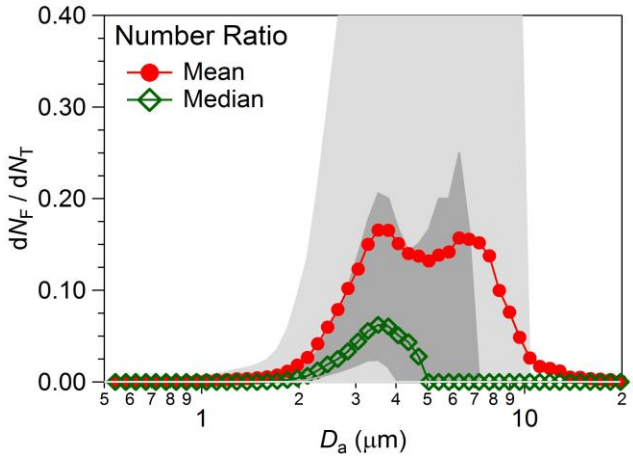

Figure 6: Size distribution of FBAP to TAP ratio averaged over the entire measurement period carried out at Munnar ($dN_F/d\log D_a = dM_F/d\log D_a$). Lower and upper parts of dark and light shaded area represents the 5^{th}, 25^{th}, 75^{th}, and 95^{th} percentile respectively.

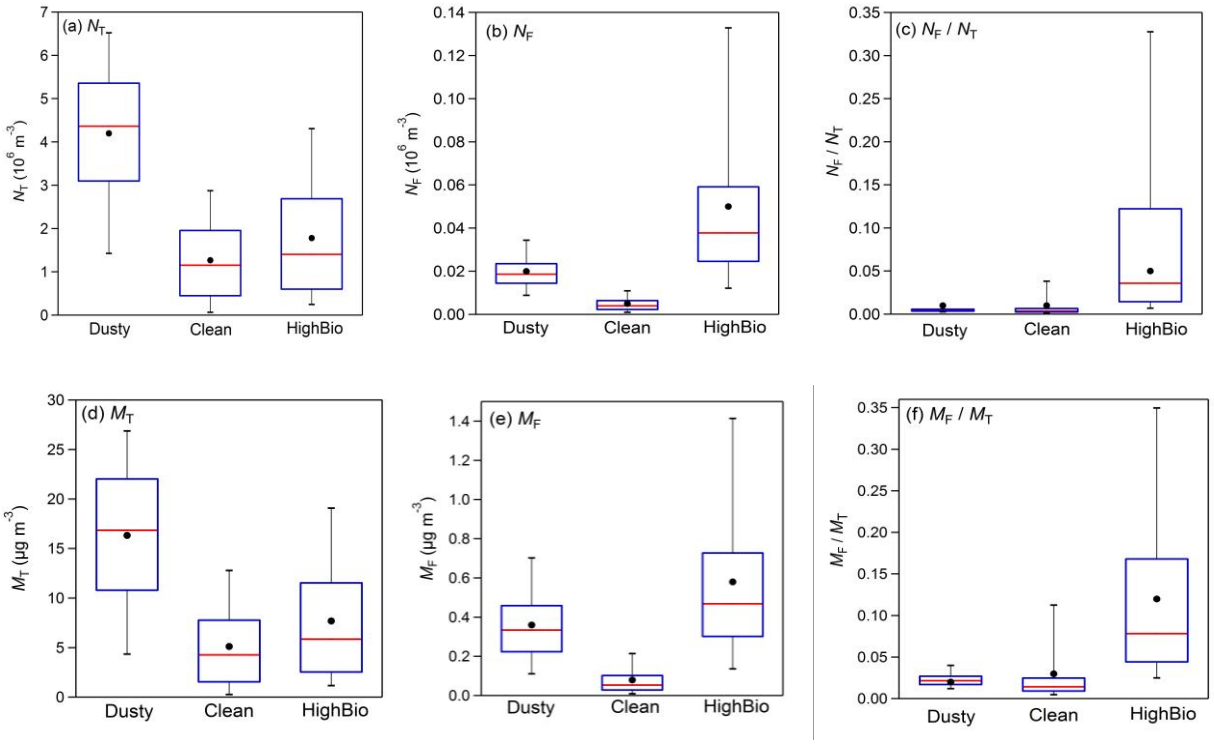

Figure 7: Statistical distribution of integrated (~1 – 20 μm) FBAP and TAP number and mass contribution of N_F to N_T, and M_F to M_T averaged over each distinct focus periods (dusty, clean, and high bio; please refer to the text for definitions related to each focus period) measurements carried out at Munnar as box whisker plots: (a) TAP number concentration (N_T), (b) FBAP number concentration (N_F), (c) contribution of FBAP number concentration to TAP number concentration (N_F/N_T), (d) TAP mass concentration (M_T), (e) FBAP mass concentration (M_F), and contribution of FBAP mass concentration to TAP mass concentration (M_T/M_F).

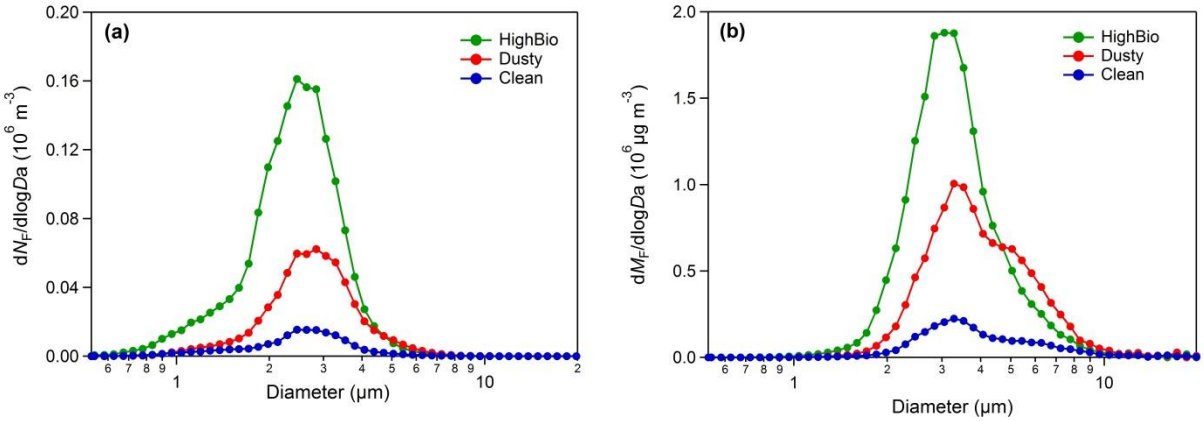

Figure 8: FBAP number (dN_F/dlog D_a) and mass (dM_F/dlog D_a) size distribution averaged over each distinct focus periods during the measurement campaign carried out at Munnar. (a) number size distribution, and (b) mass size distribution.

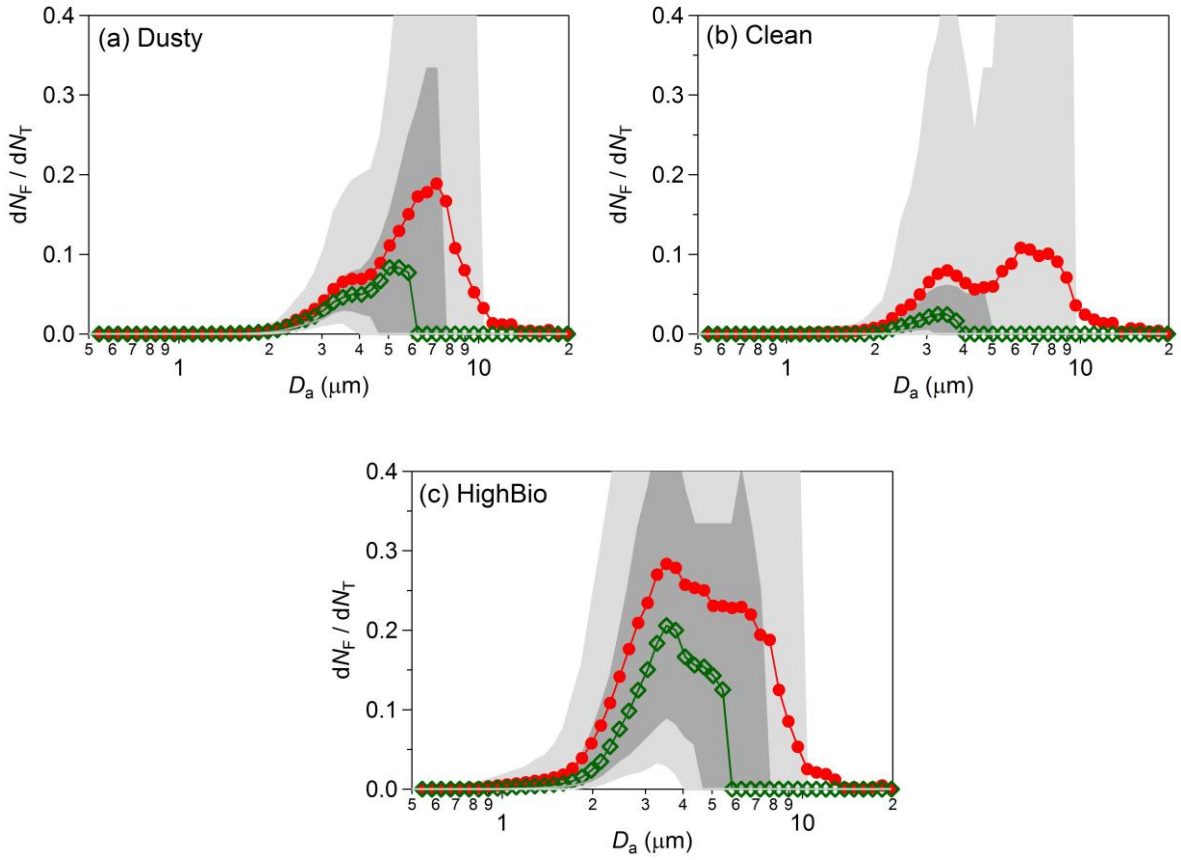

Figure 9: Size distribution of FBAP to TAP ratio averaged over the each distinct focus periods during the measurements carried out at Munnar ($dN_F/d\log D_a = dM_F/d\log D_a$). Lower and upper parts of dark and light shaded area represents the 5th, 25th, 75th, and 95th percentile respectively: (a) dusty, (b) clean, and (c) high bio.

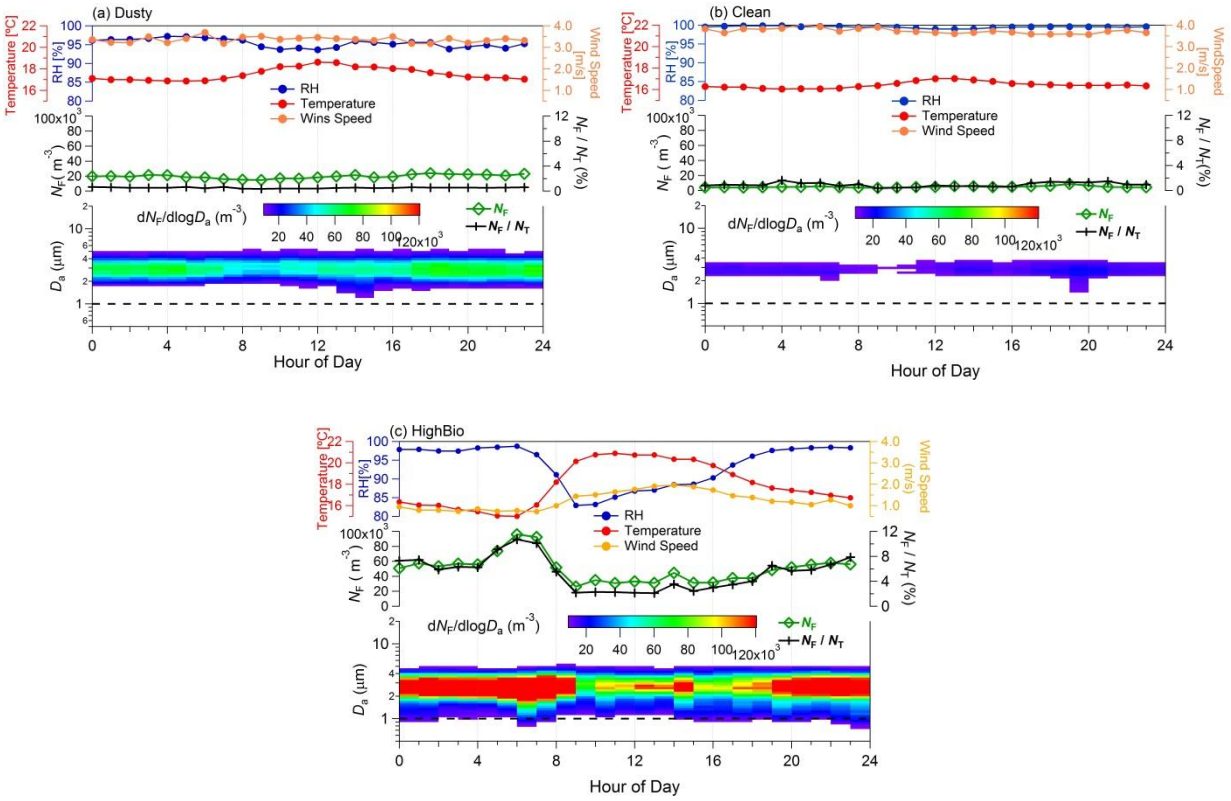

Figure 10: Diurnal cycles of observed meteorological parameters, FBAP number concentrations (N_F) and size distributions averaged over each distinct focus period identified during measurements carried out at Munnar (hourly mean values plotted against the local time of the day). Upper portion of each panel shows the observed meteorological parameters: relative humidity (%; blue), temperature (°C; red), and wind speed (m s^{-1}; orange on right axis). Middle panel shows integrated FBAP number concentration (~1 – 20 µm; N_F) on the left axis (green color) and FBAP fraction of TAP number (N_F/N_T) on the right axis (black color). Lower portion of each panel FBAP number size distribution (3-D plot) plotted against hour of the day on x-axis, aerodynamic diameter on y-axis and color is scaled for DN_F/dlog D_a indicates the concentration. Dashed black lines in lower portion of the each panel at 1.0 µm shows the particle size cut-off diameter below which fluorescent particles were not considered as FBAP due to potential interference with non-biological aerosol particles. (a) dusty (b) clean, and (c) high bio. Please refer to supplementary Figs. for corresponding TAP plots.

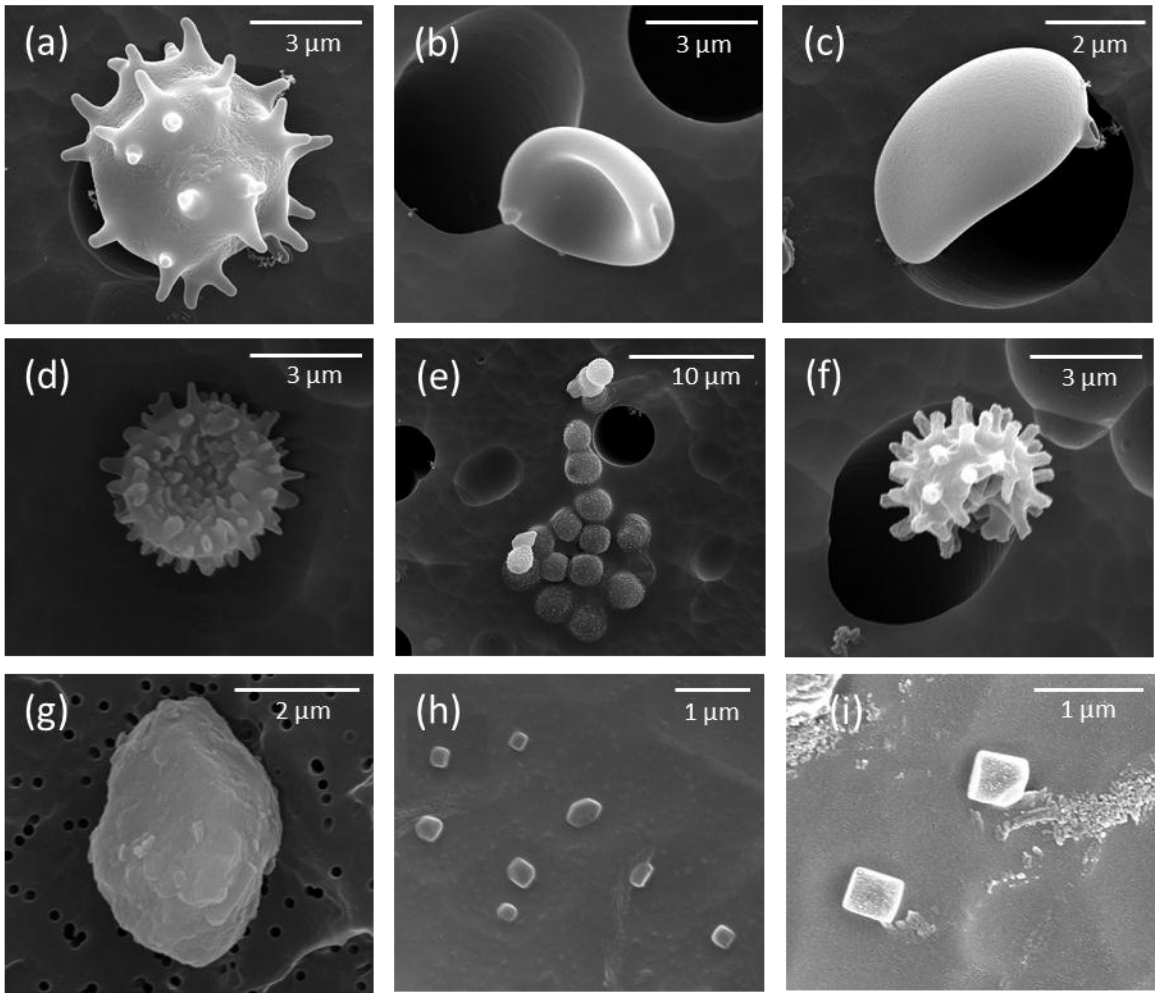

Figure 11: Scanning electron microscope images of the exemplary aerosol particles (FBAP and TAP) observed during the campaign at Munnar. The scale bar is shown at the top right corner of each image.

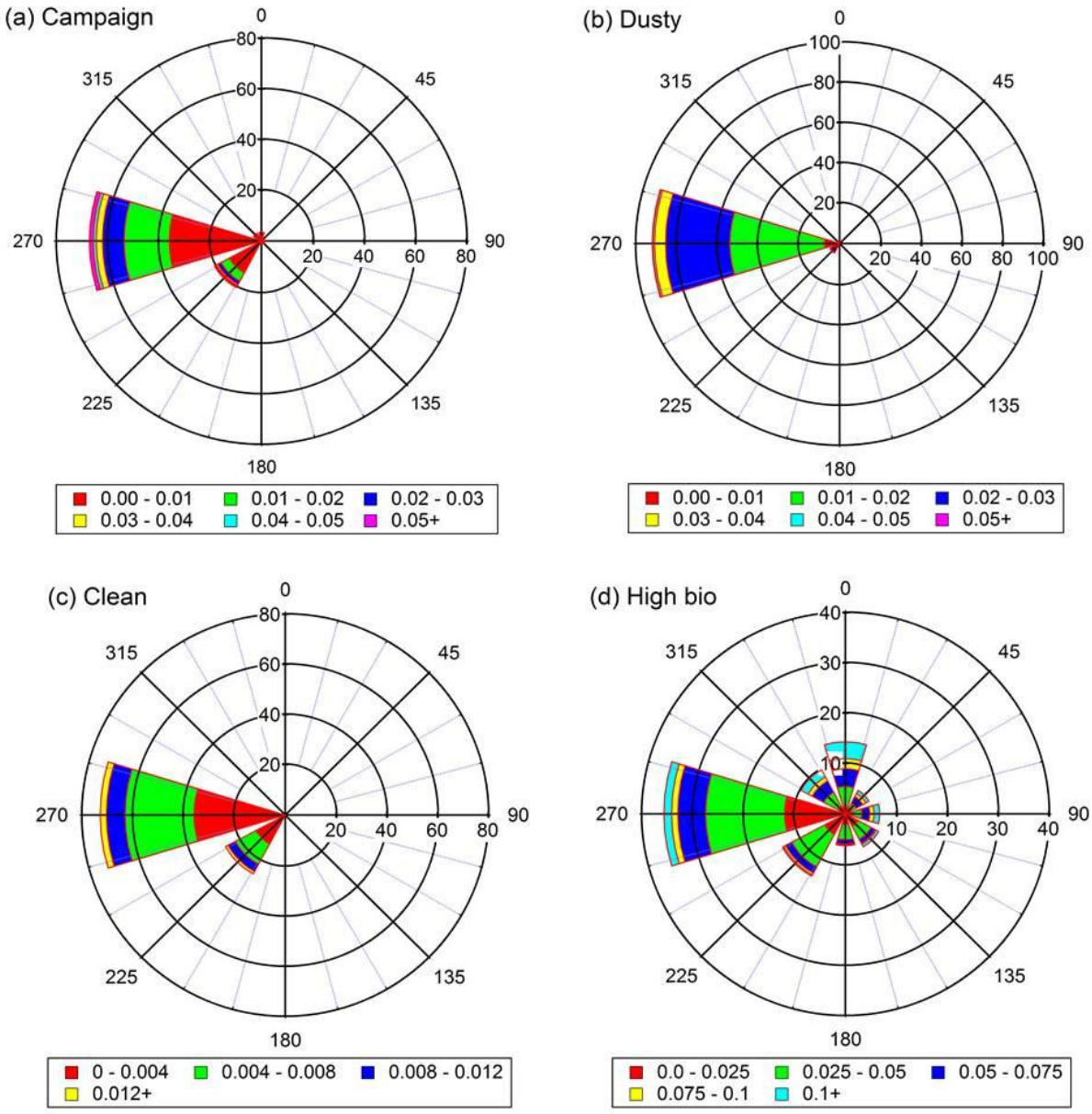

Figure 12: Wind rose diagram scaled over FBAP number concentration (N_F). These diagrams in a way are similar to the traditional wind rose diagram except representing the N_F in this case instead of wind speed. These diagram can be nominally interpreted as followed: For example (a) shows that ~52% of frequency of occurrence of N_F concentration in the range of 0 – 0.01 cm^{-3} was associated with Westerly/Southwesterly winds and on the contrary (d) indicates that out ~18% of frequency of occurrence of high concentration (N_F>0.1 cm^{-3}) ~16% was associated with Northerly/Northwesterly winds. (a) entire campaign, (b) dusty period, (c) clean period, and (d) high bio period. Note that non-uniform scale of each panel has unit of cm^{-3}.

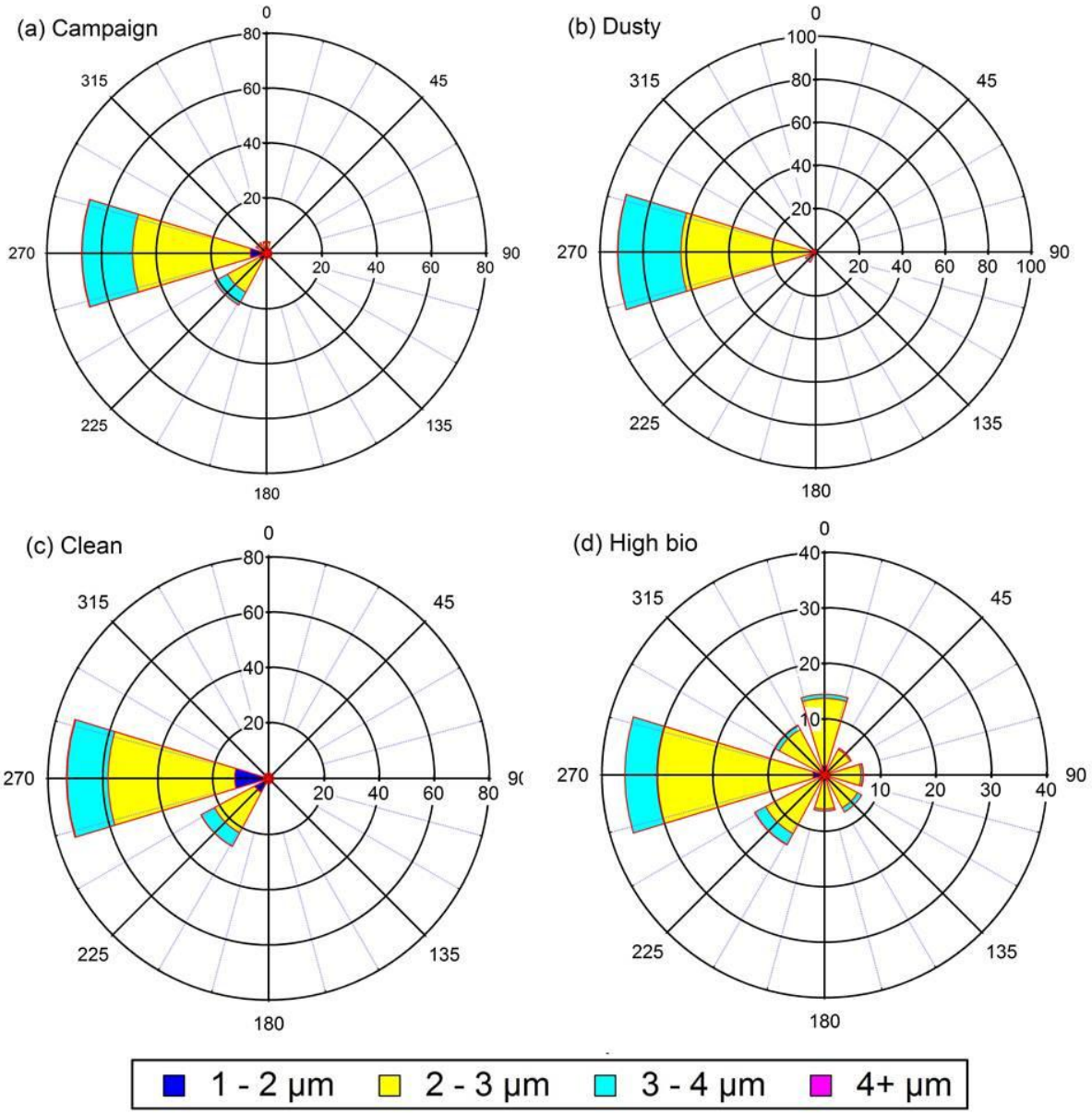

Figure 13: Same as Fig. 13 but scaled by geometric mean diameter (D_g) of dN_F/dlog D_a. (a) entire campaign, (b) dusty period, (c) clean period, and (d) high bio period.

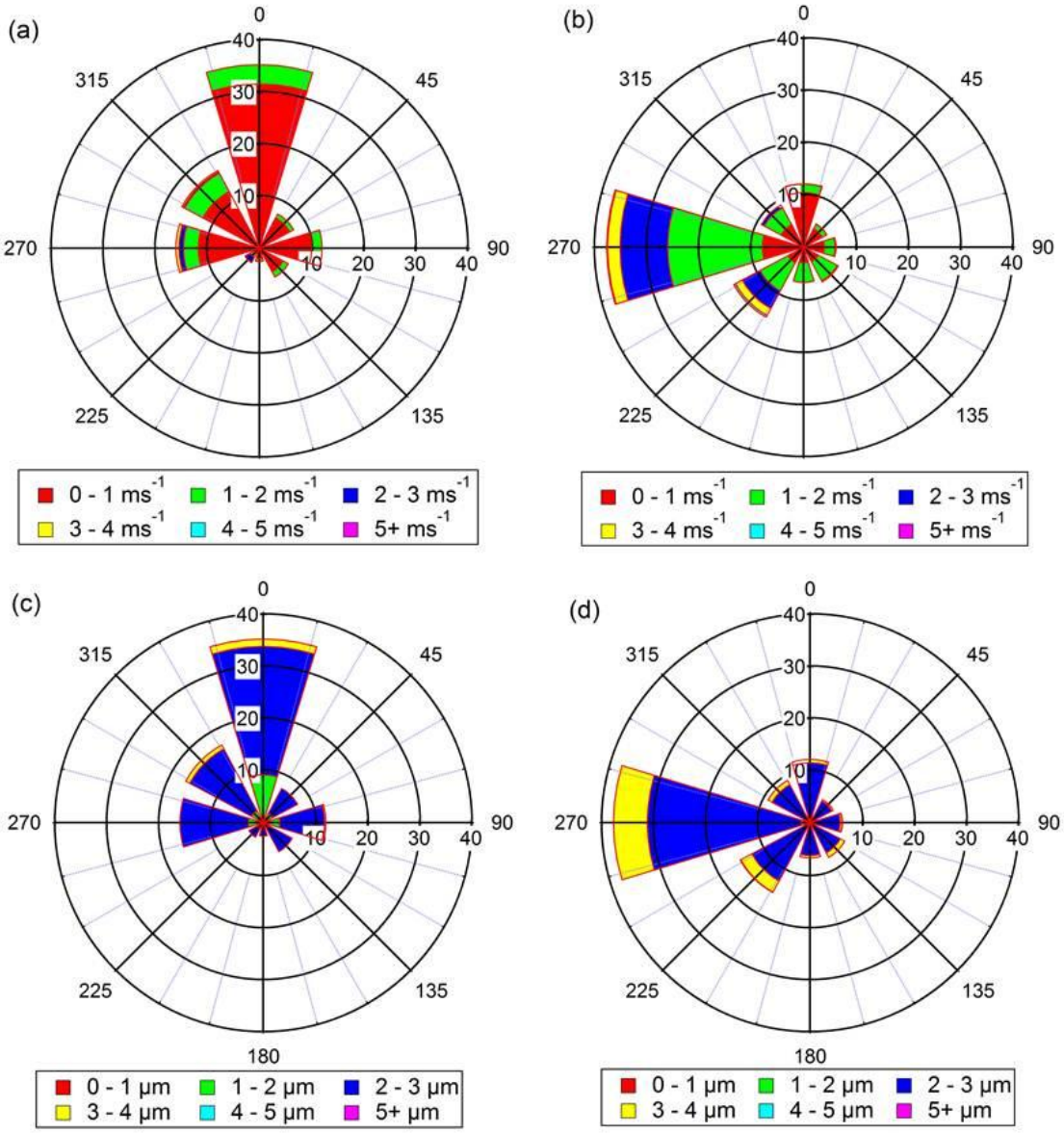

Figure 14: Wind rose diagram scaled by wind speed and geometric mean diameter (D_g) of dN_F/dlog D_a. The figures have been separated for FBAP number concentration (N_F) range, N_F >0.1 cm^{-3} and N_F< 0.1 cm^{-3} observed during high bio period. For example: when, N_F>0.1 cm^{-3} ~60% of the time wind was observed to be in the range of 0 – 1 m s^{-1} (a) and ~94% of the time the geometric mean diameter (D_g) of dN_F/dlog D_a was in the range of 2 – 3 µm (c). On the other hand for N_F<0.1 cm^{-3} ~60% of the time wind was greater than 1 m s^{-1} (b), and ~80% of the time geometric mean diameter (D_g) of dN_F/dlog D_a was in the range of 2 – 3 µm (d).

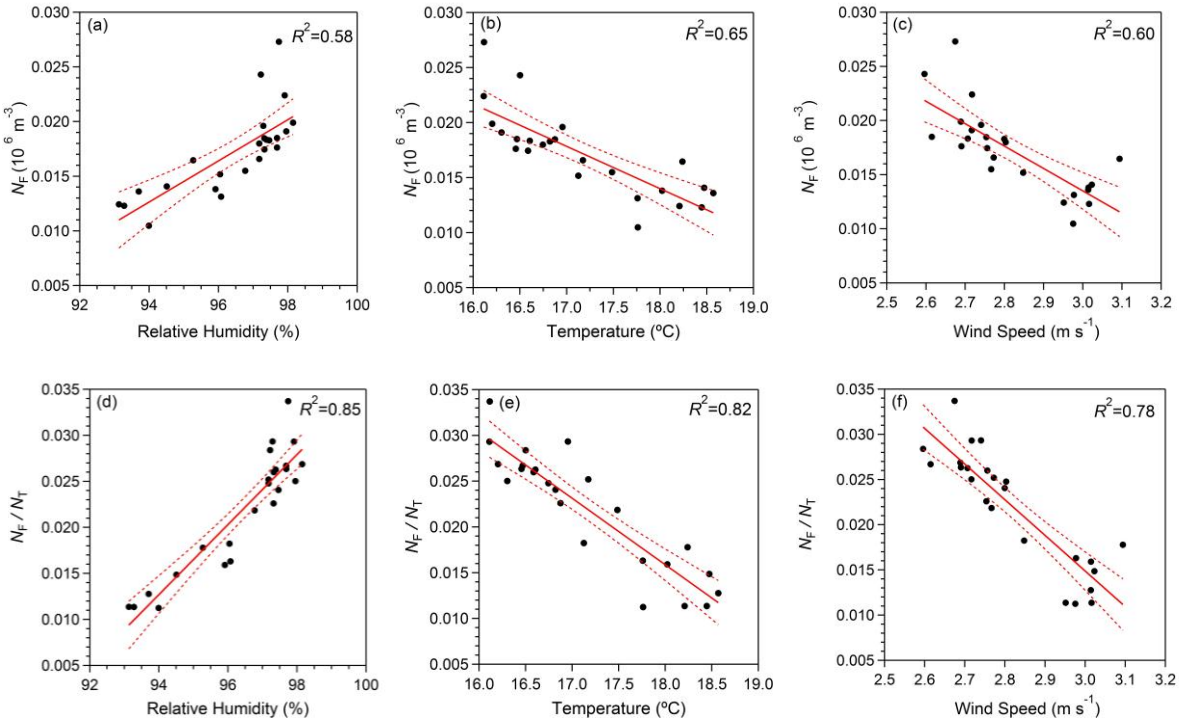

Figure 15: Correlation between aerosol particle number concentrations (N_F, N_T, and N_F/N_T) and meteorological parameters (relative humidity, temperature, and wind speed). Red line indicates the best fit to the scattered points and dashed black line indicates the 95% confidence level obtained for the best fit.